

Estimating Uncertainty Intervals from Collaborating Networks

Tianhui Zhou

TIANHUI.ZHOU@DUKE.EDU

*Department of Biostatistics and Bioinformatics
Duke University
Durham, NC 27705, USA*

Yitong Li

LYT91222@OUTLOOK.COM

*Department of Electrical and Computer Engineering
Duke University
Durham, NC 27705, USA*

Yuan Wu

YUAN.WU@DUKE.EDU

*Department of Biostatistics and Bioinformatics
Duke University
Durham, NC 27705, USA*

David Carlson

DAVID.CARLSON@DUKE.EDU

*Departments of Civil and Environmental Engineering, Biostatistics and Bioinformatics, Electrical and Computer Engineering, and Computer Science
Duke University
Durham, NC 27705, USA*

Editor:

Abstract

Effective decision making requires understanding the uncertainty inherent in a prediction. In regression, this uncertainty can be estimated by a variety of methods; however, many of these methods are laborious to tune, generate overconfident uncertainty intervals, or lack sharpness (give imprecise intervals). We address this challenge by proposing a novel method to capture predictive distributions in regression by defining two neural networks with two distinct loss functions. Specifically, one network approximates the cumulative distribution function, and the second network approximates its inverse. We denote this method Collaborating Networks (CN). Theoretical analysis demonstrates that a fixed point of the optimization is at the idealized solution, and that the method is asymptotically consistent to the ground truth distribution. Empirically, learning is straightforward and robust. We benchmark CN against several common approaches on two synthetic and five real-world datasets, including forecasting A1c values in diabetic patients from electronic health records, where uncertainty is critical. In the synthetic data, the proposed approach essentially matches ground truth. In the real datasets, CN improves results on many performance metrics, including log-likelihood estimates, mean absolute errors, coverage estimates, and prediction interval widths.

1. Introduction

Deep learning techniques have provided breakthroughs in a multitude of prediction problems; however, effective decision-making often requires accurate assessment of uncertainty in addition to prediction (Bellman and Zadeh, 1970). In a single continuous outcome, the conditional probability

distribution can be used more effectively in decision-making. For example, consider forecasting future lab values of diabetic patients from electronic health record data. This forecast should be used only if it is high confidence, which depends on how recent and complete the data is. Therefore, we want to build a system that faithfully quantifies its uncertainty based on the available information.

Quantifying uncertainty has a long history in statistics and has been extended into neural network frameworks (Blundell et al., 2015; Gal, 2016; Blei et al., 2017). The outputs of these systems should ideally be statistically calibrated (Mitchell and Wallis, 2011), meaning that the nominal level of uncertainty should reflect the true occurrence rate of an event. Much of the research has focused on binary classification problems, where out-of-the-box deep learning methods typically result in over-confident uncertainty quantification. In these cases, correction methods such as Platt scaling are necessary to adjust the predictions (Platt, 1999; Guo et al., 2017).

Poor calibration also hinders effective decision making in regression problems (continuous outcomes). Although various methods can estimate uncertainty for continuous outcomes such as heteroskedastic regression (Harvey, 1976), Bayesian approximate methods (Gal, 2016), ensemble methods (Lakshminarayanan et al., 2017), and quantile regression based methods (Tagasovska and Lopez-Paz, 2019; Koenker and Hallock, 2001), they can fall short due to model mis-specification, training instability, or lack of generalizability (Kuleshov et al., 2018). Adjusting for poor calibration is a challenging task in continuous outcomes, as the number of events to calibrate is essentially indefinite. Additionally, customization is common for the types of intervals (e.g., one-sided or two-sided, continuous or noncontinuous) or the proposed nominal levels of coverage (e.g., 70 %, 90 %, 95 %) used in a given application. In addition to well-calibrated predictions, it is necessary to have sharp, precise intervals. Given the same level of coverage, a sharper interval is preferred and is more informative (Pearce et al., 2018). Empirically, simultaneously ensuring sharpness and calibration is difficult as methods typically achieve sharpness by sacrificing calibration or the other way around.

In this manuscript, we introduce a new modeling framework capable of learning two networks to provide both faithful coverage intervals and sharp predictions. One of our networks attempts to learn the conditional Cumulative Distribution Function (CDF) given a collection of data observations. To help learn this network, we pair it with a second network that approximates the conditional inverse CDF. Despite the seeming similarity to an autoencoder with these paired functions, the networks must be learned with separate losses in a similar vein as the Generative Adversarial Network (GAN) (Goodfellow et al., 2014). Because these networks interact and must be consistent with one another, we denote the method Collaborating Networks (CN). We show that the desired solution (the two networks give the true conditional CDF and inverse CDF) is a fixed point of the optimization scheme and that the approach yields a stable solution with asymptotic consistency under certain model classes. In the following sections we provide theoretical analysis and demonstrate empirical performance on two synthetic datasets and five real-world datasets.

The code to reproduce the experiments is publicly available¹.

2. Related Work

Uncertainty in binary classification is relatively well-explored. In the classical logistic regression setting, the probability is usually well calibrated (Kull et al., 2017). However, deep networks become overconfident from overfitting, which can be partially addressed by the usage of normalization and weight decay (Guo et al., 2017) or by intelligently varying the inputs (Thulasidasan et al., 2019). Platt

1. <https://github.com/thuizhou/Collaborating-Networks>

scaling has been fairly effective (Platt, 1999). In this two-step method, the initial prediction is learned as p_i on the training data, and then a small reserved dataset is used to fit $q_i = \sigma(a + bp_i)$ as the calibrated probability. Another frequently used nonparametric calibration method is called isotonic regression (Zadrozny and Elkan, 2002), where the interval from 0 to 1 is binned from the pre-trained network, and the observed proportions on the data replaces the original predicted probability.

The challenge of studying continuous problems is that it often requires the modeling of the full span of the conditional distribution. Classically, the tilted loss functions in quantile regression provides a nonparametric framework to predict conditional quantile information for any given percentile $q \in (0, 1)$ (Koenker and Bassett, 1978), which has been extended into neural network frameworks to make it simultaneously mimic the full distribution over the full support (Tagasovska and Lopez-Paz, 2019). Although quantile regression has the large sample property to unbiasedly recover conditional quantile information, while it could be subject to underfitting or overfitting, which fails to calibrate empirical coverage in practice (Rodriguez and Yao, 2017). Modern uses of quantile regression could also be combined with conformal prediction to obtain finite sample calibration (Romano et al., 2019).

Bayesian Neural Networks naturally form a scheme to generate uncertainty estimates (Gal, 2016). One can draw a posterior predicted distribution based on the data we observed using sampling methods (Neal, 2012). To address computational challenges, one can approximate the Bayesian solution by introducing dropout training as an approximation to Bayesian inference (Gal and Ghahramani, 2016; Gal, 2016), by using variational inference (Blei et al., 2017), or by using stochastic gradient sampling methods (Li et al., 2016). While Bayesian approaches have nice theoretical properties, they suffer under mis-specification of the model and inability to correctly assess the posterior, resulting in mismatch between the claimed credibility and reality.

Regression schemes can be modified to generate heteroscedastic uncertainty by training networks to produce both a mean and variance estimate under a Gaussian likelihood (Nix and Weigend, 1994). This formulation can suffer from instability and is prone to overfitting, but can be enhanced by adjusting the gradient calculation and training the mean and variance model separately (Skafte et al., 2019). One could add mild perturbations to the covariate space and combine several independently trained uncertainty models either with regression or other frameworks for a more empirically stable and calibrated uncertainty estimate (Lakshminarayanan et al., 2017). Mixing or combining more underlying models provides more flexible approximation to different forms of distribution functions (Brando et al., 2019).

Finally, uncalibrated models for continuous outcomes could be calibrated in a post-hoc fashion. For example, calibrated regression is a method that fits an extra isotonic regression after an initial model has been trained (Kuleshov et al., 2018), which requires an extra validation set to form a recalibration mapping between nominal level of coverage and the empirical level of coverage. One could also add calibration as a regularization term to the loss of original uncertainty model to enforce the model to yield calibrated predictions with a certain extent of introduced inductive bias (Utpala and Rai, 2020).

Compared to these approaches, our method is unique because it provides an approximation to any family of distribution functions with Lipschitz continuity. Under this framework, it ensures calibration and is not subject to model misspecification in any Lipschitz continuous distribution. The losses give straightforward gradient calculations. It is theoretically sound with a large sample property. We prove consistency to ground truth for broad model classes. We have adopted several techniques to stabilize the model training, and we have practical evidence of its being robust to

extreme cases such as overfitting. Empirically, we can incorporate all training covariates to learn the conditional distribution function with our model that effectively generates the prediction interval for any possible quantile, which is shown to be precise and faithful in our empirical evaluations.

3. Preliminaries

Before introducing our learning methodology, we first set up the notation and network definitions.

3.1 Notation

Let X denote the input features, $X \in \mathcal{X} \subset \mathbb{R}^p$, with \mathbf{x} denoting an observed sample. We denote $Y \in \mathbb{R}$ as the continuous outcome variable with an observed values y . It is assumed to have a joint distribution function $p(Y, X)$ and an underlying conditional distribution function, $p(Y|X = \mathbf{x})$. Let $y_{(q, X=\mathbf{x})}$ denote the q 'th conditional quantile, where $\mathbb{P}(Y < y_{(q, X=\mathbf{x})} | X = \mathbf{x}) = q$. For instance, $q = 0.5$ would yield the median of the conditional distribution. $p(q)$ is a chosen distribution to generate the percentiles in $(0, 1]$.

3.2 Neural Network Approximation Functions

The proposed method is based on jointly learning two functions. We will first define the functions along with their predictive goals. We define a function $f_\theta(X, q)$ with parameters θ , which will be denoted as f for simplicity. The goal of this network is to approximate the inverse conditional CDF or quantile function of $Y|X$. An optimal function f should have the property that $f(q, X) = y_{(q, X)} \forall q \in (0, 1], X \in \mathcal{X}$. We then define second function as $g_\gamma(y_{(q, X)}, X)$ with parameters γ (simplified as g) that tries to approximate the conditional CDF. It can take any random value z , together with covariate information X , to predict where z is located in the full outcome space, $\mathbb{P}(Y < z|X)$. A perfect g should have the property $g(y_{(q, X)}, X) = q, \forall X \in \mathcal{X}, q \in [0, 1)$. When both f and g perfectly match their goals, they satisfy the following properties that $\forall q \in (0, 1)$

$$g(f(X, q), X) = q. \tag{1}$$

This property states that concatenating a well-learned CDF and inverse CDF function should produce an identity function. This identity is essential in connecting the two functions and their distribution properties, which will be exploited in the following to create a learning scheme.

4. Joint Function Learning

A good conditional quantile function f should have the following property to generate well-calibrated quantile estimate.

$$\mathbb{E}_{p(Y|X)}[Y < f(X, q)] \approx q. \tag{2}$$

At first glance, a straightforward approach to achieving the property in Eq. (2) would be to directly adopt it as an objective (e.g., minimize the square loss $\|\mathbb{E}_{p(Y|X)}[Y < f(X, q)] - q\|^2$); unfortunately, this objective function's gradient comes from an indicator function that is ineffective for learning the network. We bypass this learning difficulty with our joint learning scheme, but still ensure the property in Eq. (2) is properly satisfied when our framework is optimized.

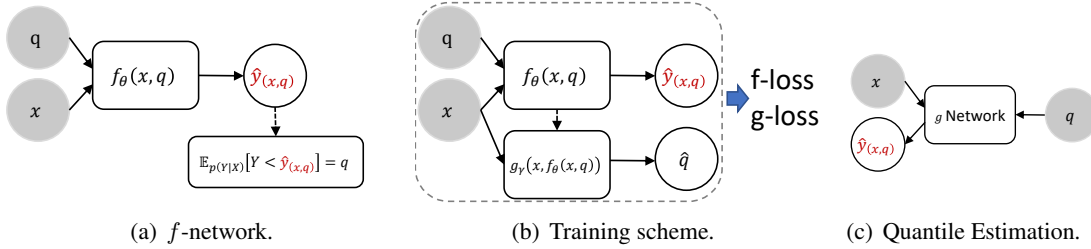


Figure 1: Illustration of CN framework. 1(a) describes training for a conditional quantile $\hat{y}(x, q)$ directly as the objective function to ensure calibration. However, the dashed arrow implies that the objective function does not produce a useful gradient. 1(b) gives the g -network, which helps with the non-derivative objective function in Eq. (2). In this framework, g and f are jointly trained to learn the CDF and conditional CDF, and they are connected by Eq. (1). 1(c) gives the final mapping to generate the conditional quantiles after the network has been trained.

Specifically, the neural networks f_θ and g_γ are bestowed with two distinct losses,

$$\text{g-loss}_\gamma : \mathbb{E}_{q \sim p(q), \mathbf{x}, y \sim p(X, Y)} [\ell(1_{(y < f_\theta(q, \mathbf{x}))}, g_\gamma(f_\theta(q, \mathbf{x}), \mathbf{x}))] \quad (3)$$

$$\text{f-loss}_\theta : \mathbb{E}_{q \sim p(q), \mathbf{x} \sim p(X)} [(q - g_\gamma(f_\theta(q, \mathbf{x}), \mathbf{x}))^2]. \quad (4)$$

The loss ℓ is a binary cross-entropy loss (or logistic loss), $\ell(b, a) = -b \log a - (1 - b) \log(1 - a)$. Eq. (3) and (4) are the losses in expectation; in practice, we would use empirical risk minimization approach. The distribution for quantiles $p(q)$ can be chosen as desired. Any distribution that fully covers the $(0, 1)$ percentile space satisfies our theoretical framework; in practice, we choose $Unif(0, 1)$ (uniform distribution). A visualization of this proposed model framework is given in Figure 1. Remarkably, under conditions similar to the theoretical claims in GANs (Goodfellow et al., 2014), these losses induce a fixed point for f and g with their desired properties (see Section 4.1).

The design of this two-loss framework can be understood as follows. When g is updated to minimize the the g -loss, f is functioning as a space searching tool to help g acquire information about the distribution function over the full relevant space. We demonstrate in our theoretical analysis that f needs only to satisfy mild conditions for g to be able to learn the optimal function. However, we are still motivated to learn f to make searching the space as efficient as possible. We demonstrate this effect empirically and note that it matches concepts in contrastive learning, where efficiency is dependent on how well the generated samples match the true distribution (Gutmann and Hyvärinen, 2010). Thus, we update f to minimize Eq. (4) to learn the distribution information directly from g . Hence, g is the main function that we use to learn the distribution information from data and f is regarded as an auxiliary function that better assists g in space searching when it gets improved during the training.

The g -loss and f -loss defined in Eq. (3) and Eq. (4) are straightforward to optimize, and they are convex in function forms, which allows an alternating learning scheme with standard gradient methods. Note that most neural network architectures could be easily incorporated in this framework. We describe the full learning strategy in Section 4.2 and provide pseudo-code in Algorithm 1.

Additionally, if desired, our method could be integrated with a pretrained model and form a two-stage or post-hoc procedure. This could be viewed as training the conditional distribution function on a reduced set of variables, matching some existing strategies in calibrating outcomes.

4.1 Theoretical Results

The functions g and f should learn the conditional CDF and conditional inverse CDF of $Y|X$. Here, we explore when the loss functions in (3) and (4) will lead to these goals. Suppose that f and g have enough capacity to represent the ground truth distribution functions (a mild assumption in neural networks), then we can show that the optimal solution is a fixed point of the training scheme. Below is a sketch of proof of these claims, with a significantly more detailed proofs available in the Appendix A. We begin our analysis with g .

Proposition 1 *Assume that $f(q, X)$ is a function we use to approximate the inverse conditional CDF or conditional quantile function of $Y|X$, $\forall q \in (0, 1)$ (not necessarily optimal but satisfying mild conditions defined in Appendix A), then a g -function minimizing (3) is optimal when it is equivalent to the CDF, or $Y|X \rightarrow_d g(Y, X)$*

Proof [Sketch of Proposition 1] First, recall our g -loss can be expanded as:

$$\begin{aligned} & - \mathbb{E}_{q \sim p(q), \mathbf{x} \sim p(X)} [\mathbb{P}(Y < f(q, \mathbf{x}) | \mathbf{x}) \log(g(f(q, \mathbf{x}), \mathbf{x})) \\ & + \mathbb{P}(Y > f(q, \mathbf{x}) | \mathbf{x}) \log(1 - g(f(q, \mathbf{x}), \mathbf{x}))] \end{aligned} \tag{5}$$

Succinctly, by fixing any $\{q, \mathbf{x}\}$ and letting $f(q, \mathbf{x}) = z$, then the inner part becomes $\mathbb{P}(Y < z | \mathbf{x}) \log(g(z, \mathbf{x})) + \mathbb{P}(Y > z | \mathbf{x}) \log(1 - g(z, \mathbf{x}))$. For any function $f(b) = -\{a \log b + (1 - a) \log(1 - b)\}$, its unique minimum is attained when $b = a$. Therefore, $g(z, \mathbf{x})$ is optimal when: $g(z, \mathbf{x}) = \mathbb{P}(Y < z | \mathbf{x}) \implies Y|X \rightarrow_d g(Y, X)$. ■

The result is also robust to the distribution $p(q)$ over percentiles as long as it has support over all of $(0, 1)$. Our default choice is the uniform distribution $Unif(0, 1)$. The Beta distribution such as $\beta(0.5, 0.5)$ could as well be utilized if we want to emphasize distribution on tails. The Proposition 1 reveals an interesting result: g has a fixed point at the optimal solution even when f is not optimal. In the meantime, this raises an open ended question on how ‘sub-optimal’ an f can be to ensure such property. In practice, each conditional distribution $Y|X$ could vary on $(-\infty, \infty)$, and having f properly covering all areas in $(-\infty, \infty)$ is not realistic. Instead, we could narrow our attention to conditional distribution within certain percentile range, such as $q \in (0.001, 0.999)$. In this way each $Y|X$ is bounded, and we can always come up with a reasonable f to search the space. For example, a fixed uniform distribution $f \sim Unif(K_1, K_2)$ where K_1 is small enough and K_2 is large enough to cover the outcome space it will satisfy the assumption.

The optimality of g leads to an additional question, which is whether our estimate will actually achieve our optimal result. To do that, we sketch out a consistency proof of g that is independent of f . This assumption is critically dependent on the existing M-Estimation theory (Van der Vaart, 2000). Prior to the statement of the theorem, we need to denote some additional notation. We define any learned g to be a function δ that comes from function space Δ . We make this switch in notation because the theorem is proved in the function space rather than the parameter space of g . We make the assumption that the ground truth CDF function g_0 is included in Δ as δ_0 . Note that using this

functional space is important for the theory because two different parameter settings in g can map to the same function. Let d be a distance measurement (e.g., absolute difference in L1 or squared difference in L2).

Next, note that the g-loss of a single sample g-loss $_i$ is:

$$-[1_{(y_i < z_i | \mathbf{x}_i)} \log(g(z_i, \mathbf{x}_i)) + 1_{(y_i > z_i | \mathbf{x}_i)} \log(1 - g(z_i, \mathbf{x}_i))]$$

Let the M -estimator M_n be the n -sample average of the loss of a given, evaluated at function g : $M_n(g) = -\sum_i^n (\text{g-loss}_i) / n$ and $M(g) = -E(\text{g-loss}_i)$ (true expectation). With that, we can now state the theorem:

Theorem 2 For $\epsilon > 0$, If the following three conditions are satisfied, then $d(\delta_0, \hat{\delta}_n) \rightarrow_P 0, n \rightarrow \infty$,

1. $\sup_{\delta \in \Delta} |M_n(\delta) - M(\delta)| \xrightarrow{Pr} 0$
2. $\sup_{\delta: d(\delta, \delta_0) > \epsilon} M(\delta) < M(\delta_0)$
3. The sequence of estimator $\hat{\delta}_n$ satisfy $M_n(\hat{\delta}_n) \geq M_n(\delta_0) - o_P(1)$

To show that our optimal finite sample estimator is consistent ($\hat{g}_n \rightarrow g_0$, the ground truth conditional CDF (δ_0 in theorem)), we need to satisfy these three conditions. A detailed derivation can be found in Appendix A, but we will give some intuition on the conditions. Note that in our derivations we limit the function class to those that satisfy Lipschitz continuity in order to satisfy these conditions. Lipschitz continuity can be imposed in neural networks (Arjovsky et al., 2017) and is a realistic assumption in many uncertainty quantification problems because of the smoothness over q . The main idea of consistency proof is to link the function proximity $\delta \rightarrow \delta_0$ through their proximity in the evaluated objective $M(\delta) \rightarrow M(\delta_0)$. The first condition is a form of uniform convergence in probability, and describes that the finite sample objective function should well-approximate the objective function in expectation as the number of samples increases regardless of the chosen δ . The second condition states that the ground truth δ_0 is the only setting that maximizes the objective function in expectation. The third condition states that we should have a sequence of functions $\hat{\delta}_n$ (estimator) estimated at each finite sample of size n , that approximately equals δ_0 in the the evaluation of finite sample objective M_n . Then by the large sample property of condition one, the limit of the sequence will dominate the objective function in expectation. Thus, if the $\hat{\delta}_n$ is not consistent proximal to ground truth, it violates these conditions.

Succinctly, for our smooth model class, our estimator g is consistent. While we assume that the optimization will be optimal in the proof, recent theoretical advances in deep learning suggest that it may be a reasonable assumption in practice (Du et al., 2018), which covers related model setups.

Next we explore the fixed point properties on f :

Proposition 3 When the g -function is ideal, then the f -function is optimal under Eq. (4). The optimum is attained when f captures the inverse CDF, i.e. $f(U, \mathbf{x}) \rightarrow_d Y | X$ given $U \sim \text{Unif}(0, 1)$.

Proof [Sketch of Proposition 3] For an ideal g -function, $g(z, \mathbf{x}) = \mathbb{P}(Y < z | \mathbf{x}) \implies g(f(q, \mathbf{x}), \mathbf{x}) = \mathbb{P}(Y < f(q, \mathbf{x}) | \mathbf{x})$. Including this in our f -loss gives

$$\min_{\theta} \mathbb{E}_{q \sim p(q), \mathbf{x} \sim p(X)} [(q - g_{\theta}(f_{\theta}(q, \mathbf{x}), \mathbf{x}))^2] = \min_{\theta} \mathbb{E}_{q \sim p(q), \mathbf{x} \sim p(X)} [(q - \mathbb{P}(Y < f_{\theta}(q, \mathbf{x})))^2]$$

If we make $q = \mathbb{P}(Y < f(q, \mathbf{x})|\mathbf{x})$, then f -loss= 0 and the loss is optimal. Let the distribution of $Y|\mathbf{x}$ be represented as F_x . Then we have $q = \mathbb{P}(Y < f(q, \mathbf{x})|\mathbf{x}) \implies q = F_x(f(q, \mathbf{x})) \implies F_x^{-1}(q) = f(q, \mathbf{x}) \implies F_x^{-1}(q) = f(q, \mathbf{x}) \implies f(q, \mathbf{x}) \rightarrow_d Y|X$. \blacksquare

By combining Proposition 1 and 3, it is clear that our ideal functions are a fixed point when we have access to the complete data distribution and our learned functions have enough complexity. We note that Proposition 3 is that it relies on g to be optimal. However, since f does not need to be optimal for g to learn effectively, we are satisfied with getting f close to the true distribution to more efficiently search the space.

As a final note, since our theory is more robust on g than it is for f , we expect that using g to capture uncertainty will perform better, which is also verified empirically in Section 5. Using f , though, is still a competitive solution, demonstrating that both networks are effectively learned with these losses.

4.2 Learning Initialization and Stabilization

As demonstrated in our theoretical results, the learning of the g -function has a fixed point at the optimal solution as long as the f -function possesses some mild properties. Moreover, a better f would help more efficiently learn g . Therefore, we want to ensure a reasonable initialization. Second, we note that f can collapse if g becomes “too good” (100 % prediction confidence), as the loss of f is embedded in g . Therefore, we want to ensure that g is initialized properly and stays stable to prevent the f function from experiencing mode collapse (Creswell et al., 2018; Salimans et al., 2016).

For the initialization, we start by training g independently of f , also known as the pre-training step. Instead of using $f_\theta(q_i, \mathbf{x}_i)$ to randomly generate samples from the conditional distribution, we adopt a generator $p(Z)$ with enough variability to help g conduct some initial explorations of the distribution in the whole outcome space. As is shown in the theory, the space searching tool $p(Z)$ does not change the optimal value of g in expectation, so this is a reasonable initialization technique. Here, we pick $p(Z)$ to be a uniform distribution ranging below the smallest and above the largest observed outcome $U(\min(y) - K, \max(y) + K)$, such that $z \sim p(Z)$. Large and positive K enforces the initial exploration of g on a larger space. It could also be chosen as the marginal empirical distribution of outcomes, as long as enough variability is involved. This pre-training step adopts the following loss:

$$- \mathbb{E}_{z \sim p(Z), y, \mathbf{x}} [1_{(y_i < z_i | \mathbf{x}_i)} \log(g(z_i, \mathbf{x}_i)) + 1_{(y_i > z_i | \mathbf{x}_i)} \log(1 - g(z_i, \mathbf{x}_i))]. \quad (6)$$

After g is pre-trained, we use the property described in Eq. (1) to robustify and stabilize the training under the full collaborating networks framework by jointly learning f and g . Specifically, for ideal functions the mapping $g(f(X, u), X) = u$ reduces the g -loss to $-[q \log(q) + (1 - q) \log(1 - q)]$ for a given q . Thus, a requirement for a well-trained network is that the output from the g function actually matches the chosen $p(q)$ distribution, which it should do in an optimally trained model. We enforce this condition by constraining the first and second moment of the logits in the g -network.

$$\begin{aligned} \text{g-loss}_\gamma : & \mathbb{E}_{q \sim p(q), \mathbf{x}, y \sim p(X, Y)} [\ell(1_{(Y < f_\theta(q, \mathbf{x}))}, g_\gamma(f_\theta(q, \mathbf{x}), \mathbf{x}))], \\ \text{s.t.} & \mathbb{E}_{q \sim p(q), \mathbf{x}, y \sim p(X, Y)} [\sigma^{-1}(g_\gamma(f_\theta(q, \mathbf{x}), \mathbf{x}))] = \mathbb{E}_{q \sim p(q)} [\sigma^{-1}(q)], \\ & \mathbb{E}_{q \sim p(q), \mathbf{x}, y \sim p(X, Y)} [(\sigma^{-1}(g_\gamma(f_\theta(q, \mathbf{x}), \mathbf{x})))^2] = \mathbb{E}_{q \sim p(q)} [(\sigma^{-1}(q))^2]. \end{aligned} \quad (7)$$

Here, $\sigma^{-1}(\cdot)$ is the inverse sigmoid function (or logit function), $\sigma^{-1}(q) = \log(q/(1 - q))$, and maps from a probability to logits. Since we define $q \sim p(q)$ as the uniform distribution in practice, these moments are straightforward to calculate as $\mathbb{E}_{q \sim \text{Unif}(0,1)}[\sigma^{-1}(q)] = 0$ and $\mathbb{E}_{q \sim \text{Unif}(0,1)}[(\sigma^{-1}(q))^2] \approx 3.29$. While at first glance, enforcing these constraints seems like it may would require a detailed optimization algorithm, it can be accomplished approximately by using the well-implemented batch normalization functions (Ioffe and Szegedy, 2015). Instead of the typical batch normalization function, it is implemented with the learned affine transformation on the output replaced by a predefined scale and shift to approximately match these idealized first and second moments. This technique forces the predicted coverage to roughly match the implied optimal distribution over q , stabilizing learning and providing additional information to the model to reduce overfitting. This regularization is another merit of learning the g , f jointly.

With these aforementioned techniques, the learning algorithm has been highly stable and robust in our empirical evaluations. This full procedure is shown in Algorithm 1.

Algorithm 1 Full Learning Algorithm

[Input]: Training samples $\{x_i, y_i\}$, for $i = 1, \dots, T$. A random generator $q \sim p(q)$ for percentile and a random generator $p(Z)$ to generate value z for space searching during the pre-training.

[Output]: Model parameters θ and γ .

[Optional] Reduce the raw covariates of X .

Pre-training to initialize g :

for iter = $1 \dots N_{pre}^{iter}$ **do**

Sample a mini-batch from training samples and generate $z_i \sim p(Z)$ for space searching.

Compute pre-train loss in Eq. (6) for g and update γ .

end for

Joint learning f and g :

for iter = $1, \dots, N^{iter}$ **do**

Sample a mini-batch of training samples and generate percentiles $q_i \sim p(q)$ for each sample.

Compute f-loss in Eq. (4) and update θ .

Compute g-loss in Eq. (3) and update γ .

end for

5. Results

In the following sections we report on our empirical simulations. We explore the impact of learning the f network in Section 5.2. We then evaluate our proposed method on synthetic data to explore its performance compared to competing methods and the optimal ground truth functions in Section 5.3. Then we compare methods on multiple real datasets in Section 5.4, showing improved performance across a variety of situations. We include three variants of CN in this experimental section to evaluate CN’s theoretical properties empirically. The first two variants come from the joint learning framework of g , f , and we denote the distributions estimated by g as “CN-g” and f as “CN-f.” The third variant is learn g with a fixed f , which is denoted as “g-only.”

Before diving into experimental details, we define the chosen comparison metrics.

5.1 Metrics

We base our uncertainty estimation evaluation on four main criteria, which are described mathematically below. First is calibration, which measures how well the predicted coverage of certain interval matches with the actual coverage. The second is sharpness, which evaluates the width of the interval. For example, if two methods both have calibrated intervals, but one method has a much smaller range of uncertainty, it is preferred. Third, we evaluate how well we capture the full conditional distribution by evaluating a discretized approximation to the conditional log-likelihood. Fourth, we evaluate prediction of the median of the data by evaluating Mean Absolute Error (MAE). We note that it is possible to evaluate Mean Squared Error (MSE) as well, but this requires averaging over the full conditional CDF. Median estimates, as evaluated by MAE, are more natural to evaluate in these methods.

5.1.1 CALIBRATION

Our quantitative calibration definition follows established literature (Kuleshov et al., 2018; Gneiting et al., 2007). A predicted nominal quantile is well calibrated when

$$\mathbb{E}_{p(Y|X)}[y_{(q_1, X)} < Y < y_{(q_2, X)}] = q_2 - q_1, \quad (8)$$

which holds $\forall 0 \leq q_1 \leq q_2 \leq 1, X \in \mathcal{X}$.

To define a metric on calibration, define the estimated interval with q (e.g. 95 %) nominal level as $I_{q,x}$ for $Y|X = x$. The miscalibration at q can be quantified as the absolute difference between q and the true probability of $Y|X = x$ falling in this interval: $|q - P_{Y|X=x}(Y \in I_{q,x})|$. In practice, only one or a few samples given $X = x$ can be observed, hence the miscalibration is aggregated over the full data, and has become a marginal concept. The miscalibration at q can be defined as follows:

$$\hat{cal}_q = |q - \sum_{i=1}^N I(y_i \in I_{q,i})/N|. \quad (9)$$

This quantity \hat{cal}_q can be evaluated and averaged over a sequence of $q_j \in \{q_1, \dots, q_M\}$ between $(0, 1]$ to evaluate calibration on the full spread of outcome distributions. The importance of each nominal level q can also vary by assigning different weights w_q , which creates a metric:

$$\hat{cal} = \sum_{j=1}^M w_{q_j} \hat{cal}_{q_j} / M. \quad (10)$$

Note that several definitions of the interval could be used; for the purpose of our study, we pick two-sided equal tail interval $[y_{q/2, X}, y_{1-q/2, X}]$ as our uncertainty objective. In empirical evaluation for \hat{cal} , we picked equally spaced 8 percentiles, with $q_1 = 0.02, q_8 = 0.98$ and all weights w_{q_j} set as 1. In some scenarios, 90% intervals are of special interest for decision making, so we also report the empirical coverage for intervals at the nominal 90% level,

$$\hat{90\%} = \sum_{i=1}^N I(y_i \in I_{0.9,i})/N. \quad (11)$$

Note that the metrics \hat{cal} and $\hat{90\%}$ do not discriminate between a marginally calibrated method and a conditionally calibrated method—both can perform well on these metrics. Thus, we require additional metrics to fully evaluate the methods.

5.1.2 SHARPNESS

At first glance, evaluating sharpness appears straightforward because a sharper method should produce narrower interval given any proposed nominal level q . However, simply reporting the interval width under any nominal level q does not form a fair standard for comparing sharpness, as it could reward some less calibrated methods which achieve sharpness by sacrificing calibration and being overconfident in interval estimate.

Therefore, we focus on making a visual approach to visualize the trade-offs between empirical coverage generated by each method, and the predicted average width.

Explicitly, given a method, for any proposed nominal level q_j , we first generate the uncertainty interval for each validation sample i with lower and upper bound $I_{q_j,i} = (l_{q_j,i}, u_{q_j,i})$. The median interval width under q_j can be represented as $width_{q_j} = med_{i=1}^N(u_{q_j,i} - l_{q_j,i})$. Then we calculate the true frequency or known as the empirical coverage value of outcomes truly covered by these intervals: $\hat{q}_j = \sum_{i=1}^N I(y_i \in I_{q_j,i})/N$. We repeat this procedure for different q_j and generate a mapping between $\{\hat{q}_j, width_{q_j}\}$. By plotting \hat{q}_j against $width_{q_j}$, we produce a curve characterizing the empirical coverage and interval sharpness. Sharp methods will correspond to a lower curve in this visualization result.

This will allow the reader to understand the sharpness with regards to the actual coverage.

5.1.3 PREDICTIVE LOG-LIKELIHOOD APPROXIMATION: GOODNESS OF FIT

In order to assess how well the predicted conditional distribution actually fits the data, a standard statistical approach is to evaluate the log-likelihood. Because the algorithms we are comparing more naturally produce intervals rather than probability density functions, this is challenging to do directly. Instead, we will use a “goodness-of-fit” (*gof*) metric that approximates the log-likelihood by using a discretization of the interval. Specifically, we discretize the real line into mutually exclusive bins B_1, B_2, \dots, B_m , and $\bigcup_i B_i = \mathbb{R}$. The discretion approximation to our log-likelihood is then given by

$$\hat{gof}(\hat{P}) = \frac{1}{N} \sum_{j=1}^m \sum_{i=1}^N I(y_i \in B_j) \log(\mathbb{P}(Y_i \in B_j | x_i)). \quad (12)$$

In all our experiment, we picked 10 bins, with $B_1 \in (-\infty, a_1]$, and $B_{10} \in (a_9, \infty)$, with a_1 and a_9 denoting the fifth and ninety-fifth percentile of the empirical distribution on Y . The intermediate bins were chosen to be equally spaced between those intervals.

Note that the log-likelihood values here will be maximized in expectation when the estimated distribution exactly matches the conditional distribution, which could also be viewed as comprehensively assessing the calibration and sharpness. Note also that the values of our \hat{gof} metric are dependent on the locations of a_1, \dots, a_9 and the number of bins; however, this is the same on all algorithms and is a fair comparison.

5.1.4 MEAN ABSOLUTE ERROR

The mean absolute error is minimized in theory if the point estimate captures the true median of the outcome. For each observation i , we estimate its conditional median $\hat{y}_{(.5, X=x_i)}$, and define the MAE as follows:

$$\text{MAE} = \sum_{i=1}^N |\hat{y}_{(.5, X=x_i)} - y_i|/N. \quad (13)$$

5.2 Impact of Learning the f -Network

Since f only needs to satisfy mild conditions for g to be able to learn effectively in the asymptotic limit, it might seem unnecessary to learn f at all

We set up a synthetic example to evaluate the impact of learning f in the finite sample case. The covariate space is a single dimension to facilitate visualizations, and we draw $N = 100$ equally spaced points between $[-0.5, 0.5] : \{x_1, \dots, x_{100}\}$. For each subject i with covariate x_i , we draw $Y_i|x_i \sim N(\sin(4\pi x_i), [0.5 + 0.3 \sin(4\pi x_i)]^2)$. The range of covariate $[-0.5, 0.5]$ covers two full periods of the trigonometric mean function, $\sin(4\pi x_i)$, and the heterogeneous error assigns larger outcome uncertainty to subjects with larger mean values. Appendix C gives the full training details.

We adopt an overparameterized neural network architectures, which creates an interpolating setting in a typically trained neural network (Belkin et al., 2019). We first demonstrate that overfitting occurs for the point predictions from the mean squared error (MSE) loss, the conditional median (QR_0.5), the conditional 25'th quantile (QR_0.25), and the conditional 75'th quantile (QR_0.75) estimated by the quantile regression. Quantile regression is designed to approximate any conditional quantile information for a given $q \in (0, 1)$. These methods all collapse to the observed outcomes and present little spread as shown in Figure 2(a).

Next, we evaluate the learned distribution for different variants of CN by comparing their estimated medians and Inter-Quantile Range (IQR) versus the ground truth. First, we set up the g -only approach with f fixed as the uniform distribution, $U(-2.5, 3, 5)$, which we denote as U-g. We do not enforce the moment matching as in Section 4.2. U-g does not collapse (Figure 2(b)), but its median and interval estimates are poor. Next, we set f to the ground truth conditional CDF. This setting is infeasible in practice, but will evaluate performance with the theoretically optimal f . We denote this case as T-g, and it gives good agreement to the ground truth, as shown in Figure 2(c). Finally, we use the full framework of CN (CN-g) by learning both functions, shown in Figure 2(d). While the performance is not quite as good as T-g in constructing sharp intervals, it is drastically better than using a suboptimal f function and more precisely predicts the spread of the true distribution.

From this setup, we see that while using a suboptimal f does not effect g in the asymptotic limit, it does in the finite sample case. Since setting f to the ground truth distribution is not realistic, it is important to adopt the collaborating structure. To address how this impacts the convergence of g to the true distribution, we set up second study to explore how these different modeling approaches match the theoretically optimal distribution (true distribution) as N increases in this generation procedure using the $g\hat{o}f$ metric. Training details can be found in Appendix C. The performances are visualized in Figure 3.

When f is the true inverse CDF, T-g stabilizes at small values of N with excellent performance. The joint learning scheme (CN-g) has only a small performance margin to when we known the inverse CDF. On the other hand, U-g's curve of $g\hat{o}f$ progresses is much slower, requiring many more samples for the same performance. In practice when the inverse CDF is unknown, the collaborating learning scheme should be preferred over a fixed f since it leads to faster convergence as a function of data samples. Note, though, that all methods converge to the ground truth distribution asymptotically, which is consistent with our theory.

5.3 Comparisons on Synthetic Data

We propose two synthetic cases to evaluate how well the Collaborating Networks recover the ground truth conditional distribution, which we denote as the theoretically optimal uncertainty

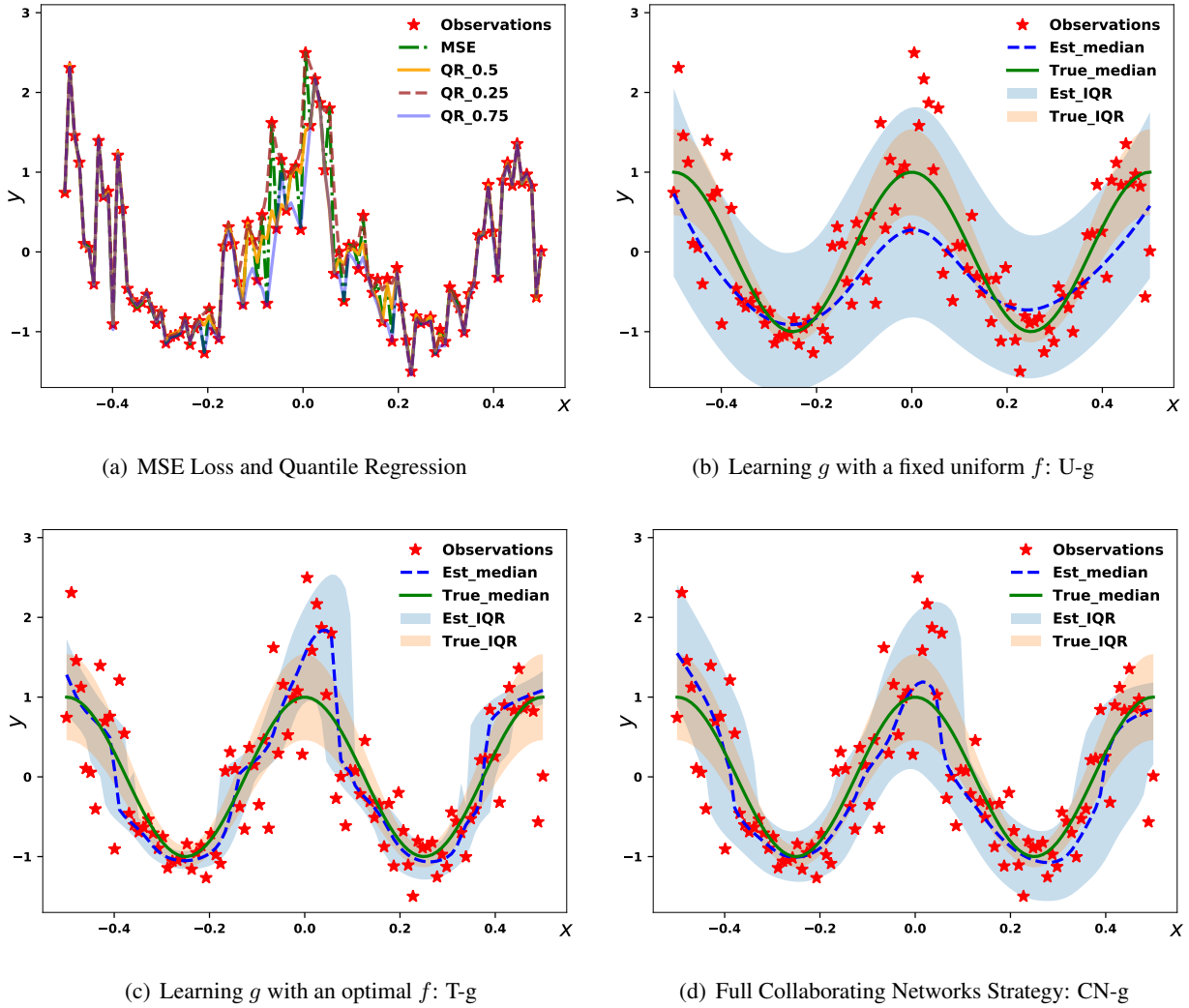


Figure 2: Visualizations of uncertainty estimates in a 1-d synthetic dataset. 2(a) shows that MSE and Quantile Regression (QR) methods essentially fit all data exactly in these settings. 2(b), 2(c), and 2(d) visualize the median and uncertainty estimate of g given a fixed f function from uniform distribution (U-g), a fixed f function from the theoretically optimal distribution (T-g), and a f function learned under collaborating networks scheme (CN-g).

estimate (TH). The first synthetic case uses a heteroskedastic Gaussian distribution, which offers scale and location transformations. The second case is simulated under the Weibull distribution that varies through scale and shape transformations.

Moreover, we assess the three variants of CN together with three other methods that are capable of estimating outcome uncertainties. The first method is MC Dropout (DP), an approximate Bayesian inference for Gaussian process assuming homogeneous outcome error (Gal and Ghahramani, 2016). The second method is the Deep Ensemble Model (EN), which is constructed by fitting and com-

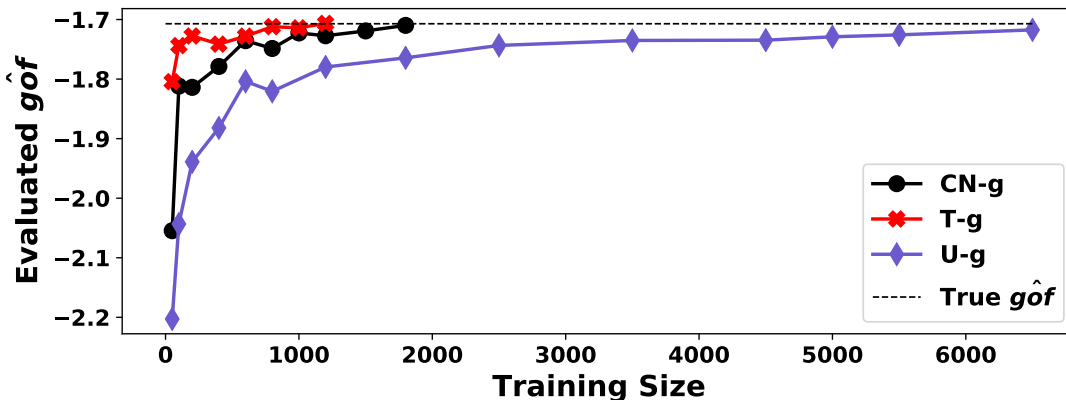


Figure 3: Visualization of $\hat{g}of$ from T-g, CN-g and U-g with varying training size.

binning five heteroskedastic regressions (Lakshminarayanan et al., 2017). The third method is the Conformalized Quantile Regression CQR, a two-step method that first estimates intervals through quantile regression and then adjusts the interval with residual errors for finite sample calibration (Romano et al., 2019). CQR is not scalable for full distribution estimation as it estimates one nominal level q at a time. Hence, CQR is skipped for $\hat{g}of$ evaluation.

We use grid search for hyper-parameter tuning for these three methods. However, we train the three variants of CN with fixed hyper-parameters across all datasets. This is to serve as an assessment of CN’s stability without careful tuning. The detailed model specification for all methods is described in Appendix C.

5.3.1 SCALE AND LOCATION SHIFT WITH A GAUSSIAN DISTRIBUTION

The first synthetic data follows a Gaussian distribution with a unique mean and variance value for each sample, $y_i \sim \mathcal{N}(\mu_i, \sigma_i^2)$. Specifically, $\mu_i \sim \mathcal{N}(0, 4)$, $\sigma_i \sim Unif(0.5, 2, 5)$, and the covariate space $x_i = [\mu_i, \sigma_i]$. We generate 700 training samples and 300 evaluation samples. This heteroskedastic Gaussian example represents an ideal setup for some of the competing methods: EN matches the correct distribution and uncertainty specification; DP provides the correct distribution form, but only slightly misspecifies the uncertainty model by assuming homogeneity. On the other hand, CN and CQR do not require any information on either distribution or uncertainty *a priori*, and they learn such information through their distribution approximations.

The empirical metrics are given in Table 1. All methods provide good marginal calibration results by having (\hat{cal}) less than 3% and the empirical coverage value for 90% intervals: $\hat{90}\%$ is close for all methods on the evaluation data. Based on these results alone, all methods are competitive. However, the $\hat{g}of$ and MAE metrics differ between the methods, revealing differences in how well they capture the distribution. Here, it is revealed that CN and EN both perform very well and essentially match the theoretically optimal distribution. Similar results hold for the MAE errors. CQR has a less competitive MAE—while has an unbiasedness property in large sample, it is not guaranteed for a finite sample approximation.

Moreover, we could assess how each method responds to the heteroskedastic variance. Under the Gaussian distribution, the optimal 90% interval scales with σ_i (Lehmann and Romano, 2006). To visualize the results, we estimate the 90% intervals for all evaluation samples and plot their

Table 1: Metrics on the heteroskedastic Gaussian synthetic data. In this case, the proposed methods CN-g and g-only essentially match the theoretical optimal values, and match the performance of EN, which assumes the correct model form.

Method	\hat{cal}	\hat{gof}	$\hat{90}\%$	MAE
TH	1.8 %	-1.65	90.0 %	1.13
CN-g	2.1 %	-1.66	91.3 %	1.13
CN-f	2.9 %	-1.71	89.0 %	1.13
g-only	2.1 %	-1.66	91.7 %	1.13
DP	2.9 %	-1.81	87.3 %	1.16
EN	0.6 %	-1.67	89.6 %	1.15
CQR	2.3 %	-	94.6 %	1.29

interval widths against the optimal interval width to evaluate whether they perfectly capture the heteroskedasticity. The result is summarized in Figure 4. Here, CN-g and CN-f visually have the best agreement with TH, as their resulting widths scatter narrowly and only deviate in the extreme widths. g-only and EN both captured the heteroskedasticity but present larger variations. CQR learns the basic trend of how uncertainty varies, but with a lot more estimation variability. Due to the assumptions in DP that each ensemble has a fixed variance, the intervals vary only slightly.

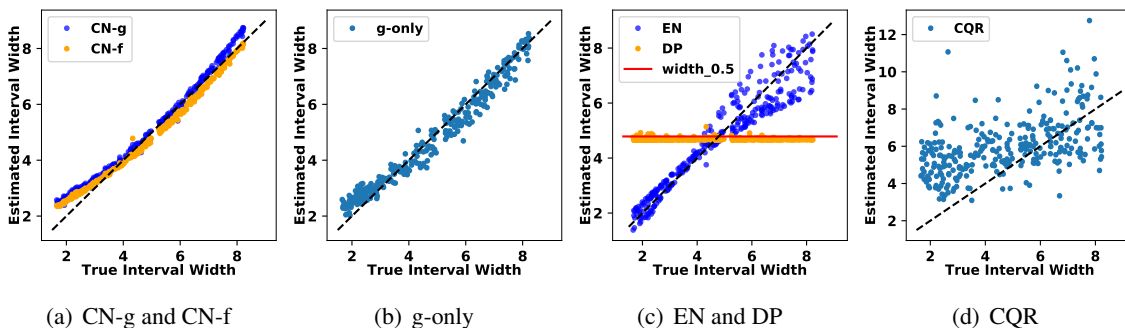


Figure 4: Scatter plot of the optimal 90 % interval widths against the estimated 90 % interval widths for all evaluation samples in the synthetic heteroskedastic Gaussian data. Points scattering closely on the 45 degree dashed diagonal line indicates a good agreement with ground truth. The full CN approach in 4(a) has overall the best agreement, whereas the competing methods do not capture the varying width as well. Note that DP 4(c) assumes a fixed variance in each ensemble model, so intervals vary only slightly.

We next further evaluate whether the estimated conditional CDF reproduces the ground truth by sketching the estimated distributions in Figure 5. Note that CN-g and g-only almost perfectly mimic the ground truth, and this holds up across a variety of input features. Except for the tail regions, CN-f

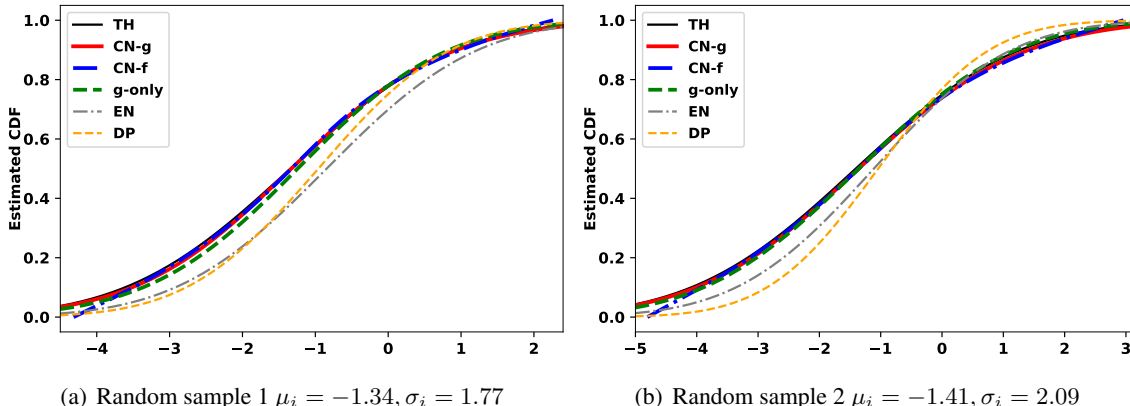


Figure 5: Visualization of the estimated CDF against the ground truth CDF (TH) for two random samples in the synthetic case 1. CN-g and g-only closely mimic the true CDF curves for both of the random samples.

provides close match to TH. Compared with the three variants of CN, EN and DP less accurately describe the distribution at individual level.

5.3.2 SCALE AND SHAPE TRANSFORMATION WITH A WEIBULL DISTRIBUTION

The second synthetic example is based on the Weibull distribution. The Weibull distribution’s support is on non-negative values and is frequently used in survival analysis to model the relationship between failure and time (Collett, 2015). The Weibull distribution has two parameters that define its scale (λ) and shape (k). Each sample y_i is generated from a Weibull distribution with a unique scale $\lambda_i \sim Unif(0.5, 2)$ and an unique shape $k_i \sim Unif(1, 5)$. The input covariates to the method are $x_i = [\lambda_i, k_i]$. We generate 700 training samples and 300 evaluation samples. Note that the Gaussian distribution can provide approximations to the Weibull distribution (Kulkarni and Powar, 2011), but they are ultimately from two different distributional families. Therefore, EN and DP are subject to model misspecifications.

Table 2 summarizes the metrics on these results. CN-g and g-only dominate the four metrics and are comparable to the ground truth (TH). EN is no longer as competitive as CN-g and g-only in this case, but due to its heteroskedastic Gaussian structure is still able to give reasonable median estimate and uncertainty estimates. In contrast, DP only estimates the median well but struggles with fair uncertainty estimates due to the non-Gaussian conditional distribution. CQR still calibrates the marginal uncertainty well, but does not accurately capture the median.

Considering the Weibull distribution’s utility in survival analysis, we additionally estimate the survival probability to compare how well each method captures the scale and shape information. Given a method, we estimate the survival probability beyond 1 ($\mathbb{P}(Y_i > 1 | X_i = x_i)$) for all evaluation samples and plot their estimates against the ground truth values. From Figure 6, we observe that CN-g has the best agreement with TH; CN-f and g-only also estimate the survival probability well, but have more variations and errors. EN performs better than DP and on average captures the survival probabilities, but suffers due to its model misspecification.

Table 2: Metrics on the Weibull synthetic data. In this non-Gaussian conditional distribution, it is clear that CN nearly matches the theoretically optimal values (TH), and methods assuming Gaussianity struggle.

Method	\hat{cal}	\hat{gof}	$\hat{90}\%$	MAE
TH	1.1 %	-1.81	88.3 %	0.37
CN-g	2.1 %	-1.84	93.0 %	0.38
CN-f	4.8 %	-2.12	84.3 %	0.38
g-only	0.9 %	-1.86	92.0 %	0.38
DP	22.8 %	-2.40	98.7 %	0.40
EN	2.9 %	-1.94	93.3 %	0.40
CQR	2.6 %	-	92.0 %	0.48

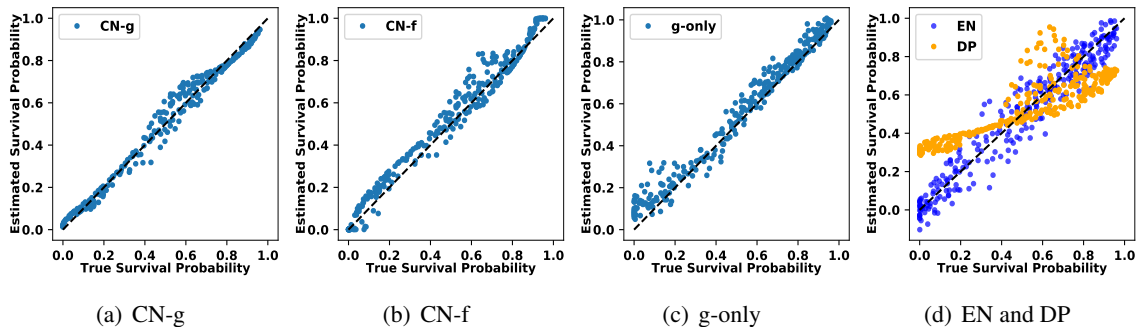


Figure 6: Scatter plot of the estimated survival probabilities, $\mathbb{P}(Y_i > 1|X = x_i)$, against the true survival probabilities on all evaluation samples in the Weibull synthetic data. Points scattering closely on the 45 degree dashed diagonal line indicates a good model fit. The full model (CN-g) provides a close fit to the true distribution 4(a). The model variants CN-f and g-only in 6(b) and 6(c) are close but comparatively less precise. EN and DP are limited by model misspecifications, shown in 6(d).

Finally, we use each method to estimate individualized survival functions (1-CDF) and plot them against the ground truth for some random drawn examples. The result is shown in Figure 7. Here, CN-g and g-only outperform the other methods, and CN-g gives closer distribution approximation in the second example than g-only. CN-f provides good estimate in the middle but not on the tails, likely due to the Weibull distribution’s heavier tail. EN and DP struggle due to model misspecification.

5.4 Comparisons on Real Data

In this section, we evaluate our method on five real data examples. In addition to the comparisons on CN, CN-f, g-only, EN, DP and CQR used in the synthetic experiments, we include calibrated regression (CR) that provides post-hoc recalibration to a trained model (Kuleshov et al., 2018). As

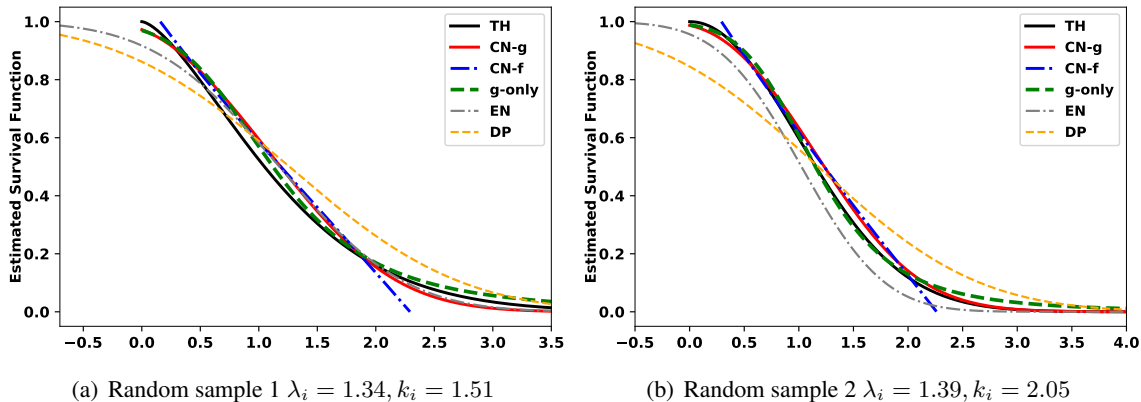


Figure 7: Visualization of the estimated survival curves (1-CDF) compared to ground truth survival curves (TH) for two random samples of the Weibull synthetic data. CN-g and g-only closely mimic the true survival curves for both of the random samples, and CN-g slightly outperform g-only in the second random example in 7(b). CN-f struggles on the tails of the distribution. EN and DP struggle as their approximations for the Weibull distribution (asymmetric) are based on a symmetric distribution (Gaussian).

DP is not always guaranteed to be well calibrated (Gal and Ghahramani, 2016), hence, we use CR as a second step for DP (DP-CR). The first four are publicly available UCI data sets² and last is an Electronic Health Records dataset. The UCI datasets are: Computer Hardware Data Set (CPU) with 209 data entries, Individual household electric power consumption Data Set (Energy) with 1441 data entries, Auto MPG Data Set (MPG) with 392 data entries, Communities, and Crime Data Set (Crime) with 1994 data entries. Energy is a time series documenting the energy measurements in a single house for 47 months, and we aggregate the outcome by days, which makes a time series of 1441 points.

The last dataset considered is an electronic health records developed from the Southeastern Diabetes Initiative (SEDI) (Miranda et al., 2013). This collection of data includes diabetic patients medical records, with the goal to forecast Hemoglobin A1c. There are records from 18,335 patients with at least 6 and at most 122 A1c measurements with additional demographic information and lab values. The measurements from individual visits were discretized to monthly entries, and a patients’ first visit was considered to occur in the 0th month, so all time stamps are time since first measurement. Electronic health records are rife with missing data and informative missingness, so recent medical-record-specific LSTM-based methods were used as the base model in all methods to address this challenge (Che et al., 2018). We use this example to demonstrate how our method can adapt to complex data structures with missing data.

In all examples, training and evaluation follows a 0.6/0.4 split. Table 3 gives the calibration results and the nominal 90 % interval coverage. CN-g outperforms other competing methods in calibrating the nominal interval coverage in 3 out of 5 cases. The variants g-only and CN-f are capable of generating intervals that have fair calibration but are less competitive. As EHR is the largest dataset, it highlights CN’s large sample property. In this substantially larger data example,

2. <http://archive.ics.uci.edu/ml/datasets>

we witness improved calibration for CN-g, CN-f and g-only. EN and CQR have consistently good calibration results in four UCI datasets. DP’s performance varies, and it fails to calibrate well enough in Energy ($\hat{cal} = 20.7\%$), CPU ($\hat{cal} = 8.1\%$) and EHR ($\hat{cal} = 7.4\%$) cases. After adjusting DP with CR (DP-CR), the overall calibration is effectively rectified.

Table 3: Quantitative calibration results on the real datasets. Each method is given ($\hat{cal} / \hat{90}\%$) on each dataset. Because the EHR data was on a secure system, it had compatibility issues with the CQR software and no result is given.

Method/Data	CPU $\hat{cal} / \hat{90}\%$	Energy $\hat{cal} / \hat{90}\%$	MPG $\hat{cal} / \hat{90}\%$	Crime $\hat{cal} / \hat{90}\%$	EHR $\hat{cal} / \hat{90}\%$
CN-g	1.8 % / 90.4 %	3.1 % / 86.1 %	1.6 % / 90.4 %	3.8 % / 85.3 %	0.6 % / 90.0 %
CN-f	6.2 % / 84.5 %	3.8 % / 82.1 %	6.3 % / 83.4 %	4.9 % / 75.4 %	1.1 % / 89.8 %
g-only	5.0 % / 94.0 %	1.2% / 89.1%	3.0 % / 91.1 %	7.4 % / 80.6 %	0.7 % / 90.7 %
DP	20.7 % / 95.2 %	8.1% / 77.3%	2.3 % / 84.1 %	7.3 % / 88.2 %	7.4 % / 88.6 %
DP-CR	4.4 % / 81.0 %	4.8 % / 82.3 %	2.1 % / 90.4 %	5.1 % / 83.7 %	0.9 % / 89.7 %
EN	2.6 % / 88.1 %	2.5% / 89.5%	2.7 % / 91.4 %	1.0 % / 87.2 %	7.3 % / 93.3 %
CQR	3.7 % / 91.7 %	1.0 % / 88.5 %	3.0 % / 96.2 %	1.5 % / 87.2 %	-

Then we turn to two model fitting metrics, as MAE reflects the accuracy for the median estimate and \hat{gof} reflects the accuracy for distribution estimate, shown in Table 4. The CN methods dominate in all datasets on these metrics, with CN-g typically the best. g-only closely follows CN-g, but loses quality without the collaborating learning scheme. CN-f is good at a median estimate, but is less so on \hat{gof} because it struggles with the tails of the distribution. DP and EN both rely on the Gaussian structure, but EN’s heteroskedasticity seems to give it more flexibility in capturing data distributions. CR efficiently re-calibrate DP via a two-step procedure. However, it is post-hoc, and is strongly dependent on the original method. Moreover, CR requires further split on the original training set for re-calibration, which could sometimes be a limitation for small data as fewer samples are employed to learn the underlying relationships. Hence CR does not necessarily augment the model fitting (\hat{gof}) in smaller data (CPU and Energy).

Table 4: Quantitative accuracy results on the real datasets. Each method is given (MAE / \hat{gof}) metric for each dataset. It is not computationally feasible to calculate \hat{gof} for CQR.

Method/Data	CPU MAE / \hat{gof}	Energy MAE / \hat{gof}	MPG MAE / \hat{gof}	Crime MAE / \hat{gof}	EHR MAE / \hat{gof}
CN-g	0.12 / -1.09	0.54 / -1.80	0.21 / -1.23	0.39 / -1.48	0.43 / -1.50
CN-f	0.12 / -1.22	0.55 / -2.07	0.23 / -1.53	0.39 / -1.90	0.44 / -1.59
g-only	0.13 / -1.09	0.53 / -1.78	0.24 / -1.24	0.41 / -1.58	0.44 / -1.51
DP	0.12 / -1.36	0.58 / -2.05	0.27 / -1.39	0.42 / -1.74	0.45 / -1.76
DP-CR	0.12 / -1.48	0.55 / -2.12	0.23 / -1.24	0.40 / -1.69	0.44 / -1.63
EN	0.16 / -1.18	0.55 / -1.82	0.25 / -1.29	0.42 / -1.68	0.45 / -1.61
CQR	0.14 / -	0.56 / -	0.27 / -	0.44 / -	-

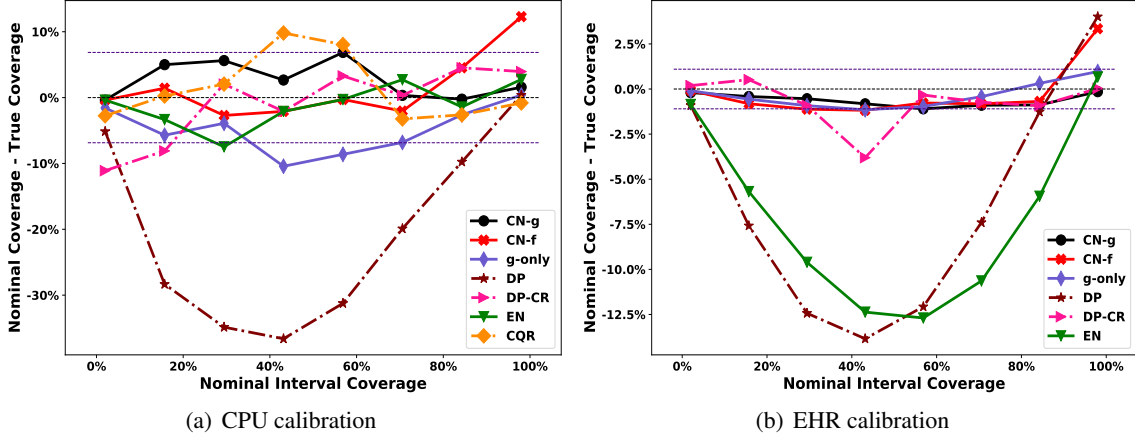


Figure 8: Visualization of the difference between the nominal and the empirical coverage for two real datasets: CPU and EHR. Curves lying closely on the 0 % horizontal line represents a good calibration result. The two other dashed horizontal lines below and above 0 % marks the maximum miscalibration of CN-g: $\max_{j=1, \dots, 8} \hat{cal}_j$, $-\max_{j=1, \dots, 8} \hat{cal}_j$. In both cases, CN-g consistently calibrates all nominal levels.

In addition to \hat{cal} , we also visualize how well a method calibrates each of the proposed nominal levels. Figure 8 summarizes the results for CPU and EHR datasets.

In these two datasets, we observe that maximum deviation from the CN-g is less than all other competing algorithms, which provides further evidence on CN’s consistency and stability in calibrating all nominal levels simultaneously. It is also shown that CN-f calibrates well at lower nominal levels but is weaker for larger nominal levels, consistent with the finding that CN-f is weaker at estimating tails. Figure 9 summarizes the interval sharpness information by plotting the true interval coverage against the median interval width for each method. A lower curve indicates that a method generate sharper intervals. In all tested situations, CN was either the sharpest or equally sharp to competing methods. Besides the evaluation on hard metric, the sharpness plot also supports CN-g’s advantage in more accurately capturing the conditional distributions in real practice, and it balancedly achieves both calibration and sharpness instead of trading one for another. We also learn from this sharpness plot that CR’s recalibration on DP does not enforce sharper intervals, which also explains that CR improves calibration but not always improves \hat{gof} . In this sense, CR is useful for matching coverage level but cannot fix poor initial predictions.

In EHR data, as the patients’ visits to hospitals are not intervalled regularly, we could further assess how each method respond to the heterogeneous visiting times. We use the 90% interval width to study heterogeneity in visiting times, since each method is able to reach approximate 90% true coverage given 90% nominal levels. For each of the following criteria on last observation time(t): $t \leq 8$; $8 < t \leq 16$; $t > 16$, we randomly select 2,000 observations and compare the estimated interval widths among different methods. The result is encapsulated in Figure 10 with boxplots. First, we notice that as times increases, the interval widths generally get larger with more spread, which indicates these models’ agreement on giving larger variability and uncertainty to the data points with increased time. Under each time, the position of CN-g’s IQR is lower than the others. It also reflects CN-g’s sharpness as it reaches approximately the same true coverage but with mostly

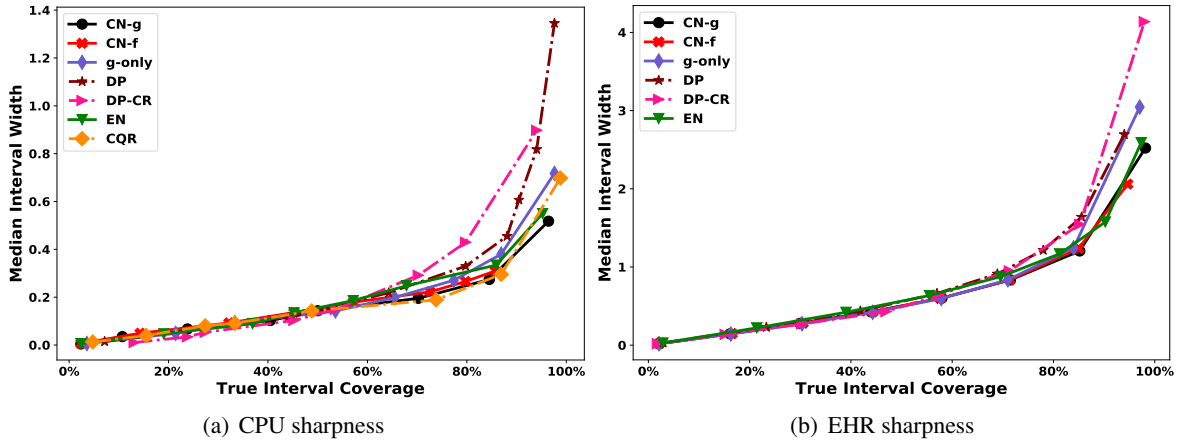


Figure 9: Visualization of the interval sharpness for two real datasets: CPU and EHR. The true coverage for every nominal level of coverage is calculated for each methods. These true coverages (x axis) are plot against the median interval widths under that true coverage level (y axis). A curve in low position can be interpreted as given a level of true coverage, it generates comparatively narrower intervals, which gives sharpness. CN-g typically generates sharper intervals for both cases.

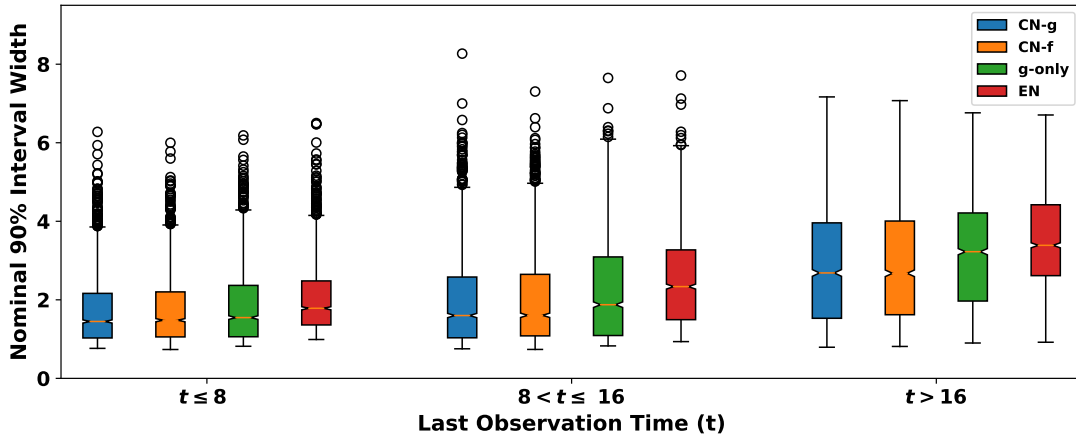


Figure 10: Visualization of the distributions of the generated 90% intervals for different last observation times(t). The x axis describes the three criteria for last observation times: $t \leq 8$; $8 < t \leq 16$; $t > 16$. For each criterion, 2,000 random observations are selected to generate the distribution of the corresponding interval widths (y axis) under each method. DP and DP-CR are not included as we examined that DP gives fairly homogeneous standard deviation estimates, of which the 95 % interval is (0.577, 0.608), and the sample variance is 0.009.

narrower intervals. Overall, the CN joint learning framework shows its capability in drawing reliable uncertainty estimate for large-scale complex data, and produce significantly sharper intervals. These uncertainty estimates can be used to derive future values for patients, and our empirical results suggest that the uncertainty intervals are highly trustworthy.

6. Discussion and Conclusion

In this paper we propose a collaborative learning scheme by simultaneously training two neural networks that characterize the CDF and inverse CDF of the conditional distribution $P(Y|X)$. In analyses of real data and synthetic data, our method showed its capability in drawing reliable uncertainty estimates from small to large-scale data with both non-temporal and temporal data structures. Empirically, our proposed method gives more accurate estimates of coverage and improved sharpness compared to the competing approaches. The method is supported by our theoretical analysis, and appears to be robust in practice. Moving forward, we will consider extensions to causal inference to model the heterogeneous treatment effect for each individual and focus on interpretable modeling.

Acknowledgments

Research reported in this manuscript was supported by the National Institute of Biomedical Imaging and Bioengineering and the National Institute of Mental Health through the National Institutes of Health BRAIN Initiative under Award Number R01EB026937.

The data used in the EHR analysis was provided by the Southeastern Diabetes Initiative (SEDI), directed by Ebony Boulware. SEDI was supported by Duke Clinical & Translational Science Award (CTSA) grant UL1TR001117; Cooperative Agreement Number 1C1CMS331018-01-00 from the Department of Health and Human Services, Centers for Medicare & Medicaid Services; and the Bristol-Myers Squibb Foundation. The data was used in accordance with Duke Health IRB Pro00025650. The EHR analysis was executed within the Duke Protected Analytics Computing Environment (PACE) supported by Duke’s Clinical and Translational Science Award (CTSA) grant (UL1TR001117), and by Duke University Health System. The CTSA initiative is led by the National Center for Advancing Translational Sciences (NCATS) at the National Institutes of Health.

The contents of this manuscript are solely the responsibility of the authors and do not necessarily represent the official views of any of the funding agencies or sponsors.

References

- Martin Arjovsky, Soumith Chintala, and Léon Bottou. Wasserstein generative adversarial networks. *International Conference on Machine Learning*, 2017.
- Mikhail Belkin, Daniel Hsu, Siyuan Ma, and Soumik Mandal. Reconciling modern machine-learning practice and the classical bias–variance trade-off. *Proceedings of the National Academy of Sciences*, 116(32):15849–15854, 2019.
- Richard E Bellman and Lotfi Asker Zadeh. Decision-making in a fuzzy environment. *Management Science*, 17(4):B–141, 1970.
- David M Blei, Alp Kucukelbir, and Jon D McAuliffe. Variational inference: A review for statisticians. *Journal of the American Statistical Association*, 112(518):859–877, 2017.

- Charles Blundell, Julien Cornebise, Koray Kavukcuoglu, and Daan Wierstra. Weight uncertainty in neural networks. *Proceedings of Machine Learning Research*, 2015.
- Axel Brando, Jose A Rodriguez, Jordi Vitria, and Alberto Rubio Muñoz. Modelling heterogeneous distributions with an uncountable mixture of asymmetric laplacians. In *Advances in Neural Information Processing Systems*, pages 8836–8846, 2019.
- Zhengping Che, Sanjay Purushotham, Kyunghyun Cho, David Sontag, and Yan Liu. Recurrent neural networks for multivariate time series with missing values. *Scientific reports*, 8(1):6085, 2018.
- David Collett. *Modelling survival data in medical research*. CRC press, 2015.
- Antonia Creswell, Tom White, Vincent Dumoulin, Kai Arulkumaran, Biswa Sengupta, and Anil A Bharath. Generative adversarial networks: An overview. *IEEE Signal Processing Magazine*, 35(1):53–65, 2018.
- Clevert Djork-Arné, Thomas Unterthiner, and Sepp Hochreiter. Fast and accurate deep network learning by exponential linear units (elus). In *Proceedings of the International Conference on Learning Representations (ICLR)*, volume 6, 2016.
- Simon S Du, Xiyu Zhai, Barnabas Poczos, and Aarti Singh. Gradient descent provably optimizes over-parameterized neural networks. *arXiv preprint arXiv:1810.02054*, 2018.
- Yarin Gal. *Uncertainty in Deep Learning*. PhD thesis, PhD thesis, University of Cambridge, 2016.
- Yarin Gal and Zoubin Ghahramani. Dropout as a bayesian approximation: Representing model uncertainty in deep learning. In *International Conference on Machine Learning*, pages 1050–1059, 2016.
- Tilmann Gneiting, Fadoua Balabdaoui, and Adrian E Raftery. Probabilistic forecasts, calibration and sharpness. *Journal of the Royal Statistical Society: Series B (Statistical Methodology)*, 69(2): 243–268, 2007.
- Ian Goodfellow, Jean Pouget-Abadie, Mehdi Mirza, Bing Xu, David Warde-Farley, Sherjil Ozair, Aaron Courville, and Yoshua Bengio. Generative adversarial nets. In *Advances in Neural Information Processing Systems*, pages 2672–2680, 2014.
- Chuan Guo, Geoff Pleiss, Yu Sun, and Kilian Q Weinberger. On calibration of modern neural networks. In *International Conference on Machine Learning-Volume 70*, pages 1321–1330, 2017.
- Michael Gutmann and Aapo Hyvärinen. Noise-contrastive estimation: A new estimation principle for unnormalized statistical models. In *Proceedings of the Thirteenth International Conference on Artificial Intelligence and Statistics*, pages 297–304, 2010.
- Andrew C Harvey. Estimating regression models with multiplicative heteroscedasticity. *Econometrica*, 44(3):461–465, 1976.
- Sergey Ioffe and Christian Szegedy. Batch normalization: Accelerating deep network training by reducing internal covariate shift. *Proceedings of Machine Learning Research*, 2015.

- Diederik P Kingma and Jimmy Ba. Adam: A method for stochastic optimization. *arXiv preprint arXiv:1412.6980*, 2014.
- R Koenker and G Bassett. Regression quantiles. *Econometrika*, 46:33–50, 1978.
- Roger Koenker and Kevin F Hallock. Quantile regression. *Journal of economic perspectives*, 15(4): 143–156, 2001.
- Volodymyr Kuleshov, Nathan Fenner, and Stefano Ermon. Accurate uncertainties for deep learning using calibrated regression. *Proceedings of Machine Learning Research*, 2018.
- HV Kulkarni and SK Powar. A simple normal approximation for weibull distribution with application to estimation of upper prediction limit. *Journal of Probability and Statistics*, 2011, 2011.
- Meelis Kull, Telmo M Silva Filho, Peter Flach, et al. Beyond sigmoids: How to obtain well-calibrated probabilities from binary classifiers with beta calibration. *Electronic Journal of Statistics*, 11(2): 5052–5080, 2017.
- Balaji Lakshminarayanan, Alexander Pritzel, and Charles Blundell. Simple and scalable predictive uncertainty estimation using deep ensembles. In *Advances in Neural Information Processing Systems*, pages 6402–6413, 2017.
- Erich L Lehmann and Joseph P Romano. *Confidence Intervals and Families of Tests*. Springer Science & Business Media, 2006.
- Chunyuan Li, Changyou Chen, David Carlson, and Lawrence Carin. Preconditioned stochastic gradient langevin dynamics for deep neural networks. In *AAAI Conference on Artificial Intelligence*, 2016.
- Marie Lynn Miranda, Jeffrey Ferranti, Benjamin Strauss, Brian Neelon, and Robert M Califf. Geographic health information systems: a platform to support the ‘triple aim’. *Health affairs*, 32(9):1608–1615, 2013.
- James Mitchell and Kenneth F Wallis. Evaluating density forecasts: Forecast combinations, model mixtures, calibration and sharpness. *Journal of Applied Econometrics*, 26(6):1023–1040, 2011.
- Vinod Nair and Geoffrey E Hinton. Rectified linear units improve restricted boltzmann machines. In *ICML*, 2010.
- Radford M Neal. *Bayesian Learning for Neural Networks*, volume 118. Springer Science & Business Media, 2012.
- David A Nix and Andreas S Weigend. Estimating the mean and variance of the target probability distribution. In *IEEE International Conference on Neural Networks*, volume 1, pages 55–60, 1994.
- Tim Pearce, Alexandra Brintrup, Mohamed Zaki, and Andy Neely. High-quality prediction intervals for deep learning: A distribution-free, ensembled approach. In *International Conference on Machine Learning*, pages 4075–4084, 2018.
- John Platt. Probabilistic outputs for support vector machines and comparisons to regularized likelihood methods. *Advances in Large Margin Classifiers*, 10(3):61–74, 1999.

- Robert N Rodriguez and Yonggang Yao. Five things you should know about quantile regression. In *Proceedings of the SAS global forum 2017 conference, Orlando*, pages 2–5, 2017.
- Yaniv Romano, Evan Patterson, and Emmanuel J Candès. Conformalized quantile regression. *Advances in Neural Information Processing Systems*, 2019.
- Tim Salimans, Ian Goodfellow, Wojciech Zaremba, Vicki Cheung, Alec Radford, and Xi Chen. Improved techniques for training gans. In *Advances in Neural Information Processing Systems*, pages 2234–2242, 2016.
- Nicki Skafte, Martin Jørgensen, and Søren Hauberg. Reliable training and estimation of variance networks. In *Advances in Neural Information Processing Systems*, 2019.
- Natasa Tagasovska and David Lopez-Paz. Single-model uncertainties for deep learning. In *Advances in Neural Information Processing Systems*, 2019.
- Sunil Thulasidasan, Gopinath Chennupati, Jeff Bilmes, Tanmoy Bhattacharya, and Sarah Michalak. On mixup training: Improved calibration and predictive uncertainty for deep neural networks. *Advances in Neural Information Processing Systems*, 2019.
- Saiteja Utpala and Piyush Rai. Quantile regularization: Towards implicit calibration of regression models. *arXiv preprint arXiv:2002.12860*, 2020.
- Aad Van Der Vaart and Jon A Wellner. Weak convergence. In *Weak convergence and empirical processes*, pages 16–28. Springer, 1996.
- Aad Van Der Vaart et al. New donsker classes. *The Annals of Probability*, 24(4):2128–2140, 1996.
- Aad W Van der Vaart. *Asymptotic statistics*, volume 3. Cambridge university press, 2000.
- Bianca Zadrozny and Charles Elkan. Transforming classifier scores into accurate multiclass probability estimates. In *ACM SIGKDD International Conference on Knowledge Discovery and Data Mining*, pages 694–699, 2002.

Appendix A. M estimator for the consistency

We start by restating Theorem 1 in Section 4.1 for an M-Estimator due to Van der Vaart (2000):

Theorem 1

For $\epsilon > 0$, if the following three conditions are satisfied, then $d(\delta_0, \hat{\delta}_n) \rightarrow_P 0, n \rightarrow \infty$

1. $\sup_{\delta \in \Delta} |M_n(\delta) - M(\delta)| \rightarrow_P 0$
2. $\sup_{\delta: d(\delta, \delta_0) > \epsilon} M(\delta) < M(\delta_0)$
3. The sequence of estimator $\hat{\delta}_n$ satisfy $M_n(\hat{\delta}_n) \geq M_n(\delta_0) - o_P(1)$

In this theorem, Δ stands for the function space Δ . δ_0 is the ground truth. M_n represents the sample average of objective as a function of δ , and M represents the expectation as a function of δ . The whole theorem to prove the consistency of estimator $\hat{\delta}_n$ is based on a maximization framework.

A.1 Marginal Consistency

We first prove the consistency of our estimating function in marginal form, without $X \subset \mathbb{R}^d$. Throughout the rest of this document we use K as a positive constant that may have different values in different situations.

A.1.1 CONSISTENCY OF g -NETWORK

Defining a Alternative Form of the Objective Function.

From g -loss, we have:

$$1_{[Y < f(q)]} \log(g(f(q))) + 1_{[Y > f(q)]} \log(1 - g(f(q))),$$

where $f(q)$ can be replaced by any $C \sim G(c)$ (a pre-defined distribution), which does not influence the consistency as long as it has support over $(0, 1)$.

We assume that the distance measurement is the cumulative probability density of C , i.e. $\mu(c) = \mathbb{P}(C \leq c)$. Based upon that, the distance between two functions can be defined as

$$d(F_1, F_2) = \left\{ \int |F_1(c) - F_2(c)|^2 d\mu(c) \right\}^{1/2}. \quad (14)$$

Then our g -loss can be re-written as:

$$- \left[(1_{[Y \leq C]} \log(g(C)) + (1 - 1_{[Y \leq C]}) \log(1 - g(C))) \right]$$

In order to use Theorem 1 to prove the function consistency, we need to transform the original minimization problem of our g -loss into a maximization problem. The new objective function is:

$$\max_g \left[(1_{[Y \leq C]} \log(g(C)) + (1 - 1_{[Y \leq C]}) \log(1 - g(C))) \right].$$

With the above objective, minimizing the g -loss is equivalent to maximizing the the objective function with respect to $M(g)$. Further, define

$$M_n(g) = 1/n \sum_{i=1}^n \left[(1_{[Y_i \leq C_i]} \log(g(C_i)) + (1 - 1_{[Y_i \leq C_i]}) \log(1 - g(C_i))) \right]$$

and

$$M(g) = E \left[(1_{[Y \leq C]} \log(g(C)) + (1 - 1_{[Y \leq C]}) \log(1 - g(C))) \right],$$

where g is the general form for a CDF function and therefore should be monotonically non-decreasing.

Defining a New Parameter Space.

In reality, with limited training samples, it is impossible to learn the full span of the distribution (i.e., we get very few samples on the tails). For inference, we are only interested in exploring a partial range, $[\phi_1, 1 - \phi_2]$ (i.e., $[0.025, 0.975]$). Assuming that there exist two real numbers *low* and *high*, such that for positive small numbers ϕ_1 and ϕ_2 , $g_0(\text{low}) = \mathbb{P}(Y \leq \text{low}) = \phi_1$ and $1 - g_0(\text{high}) = \mathbb{P}(Y > \text{high}) = 1 - \phi_2$, where g_0 is the ground truth CDF. Thus, we bound the domain of the exploring space to be within $[\text{low}, \text{high}]$, which can always be adjusted to cover the inference of interest.

Based upon the above claim, δ (function in in Theorem 1) can be further extended as any functions within the following family.

$$\mathcal{F} : \{\text{Monotonically non-decreasing } [low, high] \rightarrow [\phi_1^*, 1 - \phi_2^*]\}, \quad (15)$$

where $0 < \phi_1^* < \phi_1, 0 < \phi_2^* < \phi_2$ (that is, $\Delta = \mathcal{F}$ for Δ in Theorem 1). It is always possible to find the range, since we can choose small number or scale the variables in practice. Under this set up, since we are only interested in learning a fraction of the distribution function within a bounded domain, it is possible to define a well-behaved function to generate the output C . Specifically, we define $C \sim Unif[low, high]$, where each point is placed with equal importance, then according to Van Der Vaart and Wellner (1996), for every $r \geq 1$ (in our case $r = 1$ for the L_1 norm)

$$\mathcal{F}' : \{\text{Monotonically non-decreasing and smooth, } R \rightarrow [-1, 1]\},$$

we have

$$\log N_{[\cdot]}(\epsilon, \mathcal{F}', L_r(P)) \leq K(r)(1/\epsilon),$$

where we choose $P = \mu$, the probability measure for C . Note that $N_{[\cdot]}$ is the notation for *bracketing number*, which stands for the complexity of the family of functions (Van Der Vaart and Wellner, 1996). It is trivial to show that $\mathcal{F} \subset \mathcal{F}'$ when we restrict the domains of all functions in \mathcal{F}' to be $[low, high]$. Then we have the *bracketing number* for our function space

$$\log N_{[\cdot]}(\epsilon, \mathcal{F}, L_r(P)) \leq K(r)(1/\epsilon).$$

Therefore, $\forall g \in \mathcal{F}, \exists u_i, l_i$, s.t. $l_i \leq g \leq u_i$, where $P|u_i - l_i| \leq \epsilon$ and $i \in 1, 2, \dots, O(\exp(K/\epsilon))$. Based upon the above inequality, the new family of functions is defined as with

$$\mathcal{M} = \{m_g, g \in \mathcal{F}\}. \quad (16)$$

We can easily construct a *bracket* for this new function by bracketing m_g with

$$m_i^u = 1_{[Y \leq C]} \log(u_i(C)) + (1 - 1_{[Y \leq C]}) \log(1 - l_i(C))$$

and

$$m_i^l = 1_{[Y \leq C]} \log(l_i(C)) + (1 - 1_{[Y \leq C]}) \log(1 - u_i(C)).$$

Then by mean value theorem $|\log x| \leq K|x - 1|$, for x with positive lower bound, the probability measurement for any space (Δ, C) and measurement $P_{\delta,c}$, there is

$$\begin{aligned} P_{\delta,c} |m_i^u - m_i^l| &= P_{\delta,c} (m_i^u - m_i^l) \\ &= E \left[1_{[Y \leq C]} \log \left\{ \frac{u_i(C)}{l_i(C)} \right\} + (1 - 1_{[Y \leq C]}) \log \left\{ \frac{1 - l_i(C)}{1 - u_i(C)} \right\} \right] \\ &= E_c \left[g(C) \log \left\{ \frac{u_i(C)}{l_i(C)} \right\} + (1 - g(C)) \log \left\{ \frac{1 - l_i(C)}{1 - u_i(C)} \right\} \right] \\ &\leq K E_c [g(C) \{u_i(C) - l_i(C)\} + \{1 - g(C)\} \{u_i(C) - l_i(C)\}] \\ &= KP(u_i - l_i) \leq K\epsilon. \end{aligned}$$

Therefore, it is proved that

$$N_{[]} (K\epsilon, \mathcal{M}, L_1) = O(\exp(K/\epsilon)) < \infty.$$

Hence, our newly defined \mathcal{M} in Eq. (16) is a **Glivenko-Cantelli**, a standard approach to show uniform convergence to an objective function in expectation as evaluated in the family \mathcal{M} , and therefore **condition 1** in Theorem 1 follows naturally (Van der Vaart, 2000).

The second condition focuses on proving that the expectation of the loss function has enough separation between two different functions. Let g_0 denote the ground truth g -function, then the difference of evaluated objective function M under two function g and g_0 is

$$\begin{aligned} M(g_0) - M(g) &= E_c \left[g_0(C) \log \frac{g_0(C)}{g(C)} + \{1 - g_0(C)\} \log \frac{1 - g_0(C)}{1 - g(C)} \right] \\ &= E_c \left[g(C) \left\{ \frac{g_0(C)}{g(C)} \log \frac{g_0(C)}{g(C)} - \frac{g_0(C)}{g(C)} + 1 \right\} \right] \\ &\quad + E_c \left[\{1 - g(C)\} \left\{ \frac{1 - g_0(C)}{1 - g(C)} \log \frac{1 - g_0(C)}{1 - g(C)} - \frac{1 - g_0(C)}{1 - g(C)} + 1 \right\} \right] \end{aligned}$$

For function with form $h(x) = x \log x - x + 1$, it can be shown that for a large $Z > 0$, there exists C_Z , s.t. $h(x) > C_Z(x - 1)^2$, $0 < x < Z$. Then

$$\begin{aligned} M(g_0) - M(g) &\geq KE_c \left[g(C) \left\{ \frac{g_0(C)}{g(C)} - 1 \right\}^2 + \{1 - g(C)\} \left\{ \frac{1 - g_0(C)}{1 - g(C)} - 1 \right\}^2 \right] \\ &\geq Kd^2(g, g_0) \end{aligned}$$

where $d()$ is defined in Eq. (14). **Condition 2** follows with the above inequality.

Condition 3 is obvious if we can get the maximum likelihood estimator (MLE) \hat{g}_n with the full class defined by class \mathcal{F} in Eq. (15). In practice, we try to attain the MLE within a function class defined by neural networks, and we need to show that the maximization by neural networks still makes the condition hold. Note that based on the proof of Theorem 1 (Van der Vaart, 2000), \mathcal{F} includes both g_0 and \hat{g}_n for large n , i.e., \hat{g}_n is monotone. Hence, to guarantee this monotonicity, we further assume this class attained by neural network is a subclass of \mathcal{F} and defined by

$$\mathcal{F}^* : \{\text{Monotonically non-decreasing, attainable by neural network } [low, high] \rightarrow [\phi_1^*, 1 - \phi_2^*]\}.$$

Now, we take a detour for establishing **condition 3**. Assuming that there exists $g_n \in \mathcal{F}^*$, s.t. $M_n(g_n) > M_n(g_0) - op(1)$. Additionally, with the fact $M_n(\hat{g}_n) \geq M_n(g_n)$ when the neural networks reach the finite sample maximization, we get

$$M_n(\hat{g}_n) > M_n(g_0) - op(1).$$

Hence with all three conditions are satisfied, we can arrive at

$$d(\hat{g}_n, g_0) \rightarrow_p 0, n \rightarrow \infty$$

Now, we switch our focus to the existence of the function g_n . To simplify the argument, assume g'_0 is the true density function(the derivative of the CDF g_0) which has a positive lower

bound within $[low, high]$. From the Universal Approximation Theorem, there exists a function $g'_n(x) = \sum_i v_i \phi(w_i x + b)$ attained by neural network, s.t. $\|g'_n(x) - g'_0(x)\|_\infty < o(1)$. Then for large n , g'_n also has a positive lower bound.

Next we define $g_n = \int g'_n dx$. From this definition, it is easy to see that g_n has form $g_n(x) = \sum_i v_i \psi(w_i x + b)$, with $\psi = \int \phi$, that is, $g_n(x)$ is also attained by neural network. Besides, we have $\|g_n(x) - g_0(x)\|_\infty < o(1)$. In addition, by the fact that for any large n , g'_n also has a positive lower bound, we know that g_n is also a monotone function for any large n . This proves that $g_n \in \mathcal{F}^*$.

In the following, we will show $M_n(g_n) > M_n(g_0) - op(1)$ to finish the verification of **condition 3** and complete the proof. Since

$$|M_n(g_n) - M_n(g_0)| \leq \frac{1}{n} \sum_{i=1}^n \left| 1_{[Y_i \leq C_i]} \log \frac{g_n(C_i)}{g_0(C_i)} + (1 - 1_{[Y_i \leq C_i]}) \log \frac{1 - g_n(C_i)}{1 - g_0(C_i)} \right|,$$

and

$$\begin{aligned} \left| 1_{[Y_i \leq C_i]} \log \frac{g_n(C_i)}{g_0(C_i)} + (1 - 1_{[Y_i \leq C_i]}) \log \frac{1 - g_n(C_i)}{1 - g_0(C_i)} \right| &\leq \left| \log \frac{g_n(C_i)}{g_0(C_i)} \right| + \left| \log \frac{1 - g_n(C_i)}{1 - g_0(C_i)} \right| \\ &\leq K / \min(\phi_1^*, \phi_2^*) o(1) = o(1), \end{aligned}$$

by the fact that $|\log x| \leq K|x - 1|$ for x with positive lower bound and using the boundedness of g_0 and the fact that $\|g_n(x) - g_0(x)\|_\infty < o(1)$.

Then we know $|M_n(g_n) - M_n(g_0)| \leq o(1)$. Therefore,

$$M_n(g_n) > M_n(g_0) - op(1).$$

A.1.2 CONSISTENCY OF f

The form of f -loss determines its strong reliance on g function. This dependency shows up in both the consistency and the fixed point solution. Although we can use g function to directly solve the quantiles, we are still interested in showing that f can reach consistency under some additional assumptions.

We start by showing a stronger version of convergence of g . Previously, we have shown that g is consistent in probability, now assume that we have:

$$\sup_{c \in [low, high]} |\hat{g}_n(c) - g_0(c)| \rightarrow_p 0 \quad (\text{I})$$

When \hat{g}_n is attained, \hat{f}_n can be defined as \hat{g}_n^{-1} , which is bound to minimize the empirical f -loss, since $q = \hat{g}_n(\hat{g}_n^{-1}(q))$. The question is whether the sequence of \hat{f}_n converges to f_0 as expected.

We want to show that

$$\sup_{q \in [\phi_1^*, 1 - \phi_2^*]} |\hat{g}_n^{-1}(q) - g_0^{-1}(q)| \rightarrow_p 0$$

since g_0 is a monotonic and continuous function, its inverse g_0^{-1} is monotonic and continuous, with its domain being a compact set $[\phi_1^*, 1 - \phi_2^*]$. Therefore, it is uniformly continuous. Let's define any $q \in [\phi_1^*, 1 - \phi_2^*]$, we have $y_q = g_0^{-1}(q)$. assume that we have $\delta > 0$, s.t. when $|q - q'| < 2\delta \implies |g_0^{-1}(q) - g_0^{-1}(q')| = |y_q - g_0^{-1}(q')| < \epsilon$. Hence,

$$g_0(y_q - \epsilon) < q - \delta \text{ and } g_0(y_q + \epsilon) > q + \delta \quad (\text{II})$$

if not we have $g_0(y_q - \epsilon) \geq q - \delta$ then $|y_q - \epsilon - y_q| < \epsilon$, contradiction! same is for the second part. With (I), we also have N_1 , s.t. when $n > N_1$, we have $|\hat{g}_n(c) - g_0(c)| < \delta$. Now, let $\hat{y}_{n,q} = \hat{g}_n^{-1}(q)$. We want to show that $|y_q - \hat{y}_{n,q}| < \epsilon$.

Prove by contradiction: if $y_q - \hat{y}_{n,q} \geq \epsilon \iff y_q - \epsilon \geq \hat{y}_{n,q}$, then $g(y_q - \epsilon) > \hat{g}_n(y_q - \epsilon) - \delta \geq \hat{g}_n(\hat{y}_{n,q}) - \delta = q - \delta$, that contradicts with (II). Therefore, $y_q - \hat{y}_{n,q} < \epsilon$. The other direction can be proved similarly. Then we get $|y_q - \hat{y}_{n,q}| < \epsilon$. In this whole process, we showed that for $n \geq N_1$

$$|\hat{g}_n(y_q) - g_0(y_q)| < \delta \implies |g_0^{-1}(q) - \hat{g}_n^{-1}(q)| < \epsilon,$$

which further implies that

$$P \left(\sup_{c \in [low, high]} |\hat{g}_n(c) - g_0(c)| < \delta \right) \leq P \left(\sup_{q \in [\phi_1^*, 1 - \phi_2^*]} |\hat{g}_n^{-1}(q) - g_0^{-1}(q)| < \epsilon \right) \rightarrow 0,$$

that completes the proof.

A.2 Extension to conditional distribution

In general, we are estimating the distribution of $Y|X$, to prove the consistency of g . We still rely on the construction of M-estimator, but limited to a multivariate function family. The major difference for the general case is using the smoothness of the conditional distribution to establish a multivariate function family is a **Glivenko-Cantelli** while for the marginal case we have shown that a univariate monotone function class is a **Glivenko-Cantelli**. The detailed proof for the general case with the conditional distribution is otherwise almost the same with the previous proof and is not presented here. In the following, we only present the theorem (Van Der Vaart et al., 1996) for evaluating the *bracketing number* for a smooth multivariate function class and therefore verifying that the function class is a **Glivenko-Cantelli**.

Theorem 4 *Suppose $X \subset R^d$ to be bounded and convex with nonempty interior.*

There exists a constant K , depending only on α , diagram X , and d , s.t

$$\log N_{[]}(\epsilon, C_1^\alpha, L_r(P)) \leq K(1/\epsilon)^{d/a}$$

In terms of the convergence of f , we can still ensure that it holds for each fixed covariate $X = \mathbf{x}$. For the full covariate space of X , its convergence speed could differ given different X . However, f is used under the CN framework as an auxiliary learning function only, and forcing it to learn together with g , is to make space exploration more efficient on high density areas. In real practice, g is our choice for predicting the outcome uncertainty, which is also shown to empirically outperform f in our experiments.

Appendix B. Proofs of Additional Claimed Properties

Lemma 5 *The sampling distribution on the quantiles does not influence the optimal solution of $f(\cdot)$, and $F(U, X) \rightarrow_d Y|X$.*

Proof For g-loss and f-loss to attain its maximum, we have shown in main article that for fixed X and $q \in (0, 1]$, the optimal solution is $F_X^{-1}(q) = f(q, X)$. Replacing the sampling distribution

from $U \sim \text{Uniform}(0, 1)$ to any G , the optimal solution for each fixed $q \in (0, 1]$ is still $F_X^{-1}(q) = f(q, X), \forall q \in (0, 1]$ Therefore, for any sampling distribution imposed on q , we still have

$$F_X^{-1}(U) = f(U, X),$$

which is a perfect mimicking of the inverse CDF. \blacksquare

Lemma 6 *The optimal g and f functions do not change if $g\text{-loss} = g\text{-loss} + \text{ext}$ is used to train the g function, where $\text{ext} = \lambda E_q E_{\mathbf{x}} (q - g(f(q, \mathbf{x}), \mathbf{x}))^2$ (λ is the tuning parameter and $\lambda > 0$)*

Proof Since $\text{ext} \geq 0$, so $\min g\text{-loss} \leq \min g\text{-loss} + \text{ext}$. Using the prior fixed point optimal solution of $g(z, \mathbf{x}) = \mathbb{P}(Y < z | \mathbf{x})$, $f(q, \mathbf{x}) = y_{q, \mathbf{x}}$, we find that $E_q E_{\mathbf{x}} (q - g(f(q, \mathbf{x}), \mathbf{x}))^2 = 0$, since $g(f(q, \mathbf{x}), \mathbf{x}) = \mathbb{P}(Y < f(q, \mathbf{x}) | \mathbf{x})$, and $\mathbb{P}(Y < f(q, \mathbf{x}) | \mathbf{x}) = \mathbb{P}(Y < y_{q, \mathbf{x}} | \mathbf{x}) = q$, so $\min g\text{-loss} = \min g\text{-loss} + \text{ext}$, so $g\text{-loss} + \text{ext}$ also gets its minimization with same optimal solution. \blacksquare

Lemma 7 *$g \circ f(\hat{p}) = \mathbb{E}_{y, \mathbf{x} \sim p(Y, X)} [\log(\hat{p}(y | \mathbf{x}))]$, is minimized when the estimated conditional density $\hat{p}(y | \mathbf{x})$ matches the true density $p(y | \mathbf{x})$: $\hat{p}(y | \mathbf{x}) = p(y | \mathbf{x})$.*

Proof For any estimated density of $\hat{p}(y | \mathbf{x})$ the difference of log likelihood evaluated by $p(y | \mathbf{x})$ and $\hat{p}(y | \mathbf{x})$ can be expressed as: $D(\hat{p}(y | \mathbf{x}), p(y | \mathbf{x})) = \mathbb{E}_{y, \mathbf{x} \sim p(Y, X)} [\log(\hat{p}(y | \mathbf{x}))] - \mathbb{E}_{y, \mathbf{x} \sim p(Y, X)} [\log(p(y | \mathbf{x}))]$. It can be simplified as following:

$$\begin{aligned} D(\hat{p}(y | \mathbf{x}), p(y | \mathbf{x})) &= \mathbb{E}_{\mathbf{x} \sim p(X)} [\log(\hat{p}(y | \mathbf{x}) / p(y | \mathbf{x})) p(y | \mathbf{x}) dy] \\ &< \mathbb{E}_{\mathbf{x} \sim p(X)} \left[\log \left(\int_y \hat{p}(y | \mathbf{x}) / p(y | \mathbf{x}) \times p(y | \mathbf{x}) dy \right) \right] \text{ (Jensen's Inequality)} \\ &= \mathbb{E}_{\mathbf{x} \sim p(X)} \left[\log \left(\int_y \hat{p}(y | \mathbf{x}) dy \right) \right] = 0 \end{aligned}$$

Therefore, the true density always maximizes the expectation. \blacksquare

Appendix C. Description on Neural Network and Experimental Details

C.1 Section 5

C.1.1 LEARNING UNDER A SUBOPTIMAL SETTING

We adopt over-parameterized neural network structures and small learning rate to achieve an environment that a method can easily overfit the data. The learning rate for all methods are fixed to be $1e-5$ with ADAM optimizer (Kingma and Ba, 2014). We set the batch size to be equal to the sample size of 100 throughout all methods. The neural network structure is set to be a feed-forward network with two hidden layers both of size 1,000, and ReLU as activation function (Nair and Hinton, 2010) for

point prediction by mean squared error (MSE) loss; the conditional median (QR_0.5), the conditional 25'th quantile (QR_0.25) and the conditional 75'th quantile (QR_0.75) estimated by the quantile regression loss. For CN, the g function in this section is designed to be a feed-forward network with two hidden layers both of size 1,000 and the f function is designed to be a feed-forward network with three hidden layers all of size 1,000. The activation functions for both g and f in CN are set to be eLU (Djork-Arné et al., 2016).

C.1.2 NETWORK FOR CONVERGENCE COMPARISONS

The auxiliary function f is still set to be the ground truth for T-g, and the uniform distribution for U-g. In this case, we stop using the over-parameterized network structures. We reduced the network size for computational efficiency as a feed-forward network with two hidden layers with size of 100 and 80; and the f function is designed to be a feed-forward network with three hidden layers with size of 100, 80 and 60. The learning rate for both networks are fixed as $1e-4$. The batch size is set as 200 throughout all training sizes. In the case where training sample size is less than 200, the batch size is automatically reduced to the sample size.

C.2 Section 6

C.2.1 NETWORKS

CN: The CN-g and g-only function in this section are both designed to be a feed-forward network with two hidden layers of size 100 and 80, and the f function is designed to be a feed-forward network with three hidden layers with layer sizes of 100, 80, and 60. We set the activation function as eLU for each layer. At the end of each layer, batch normalization is used. The optimizer of all functions under the CN framework are based on ADAM with the step size fixed as $1e-4$. The batch size is set as 100.

EN: The deep ensemble model is implemented by stacking five heteroskedastic regressions. Each of them were implemented by tensorflow probability, with negative log likelihood for Gaussian distribution as its loss. It is designed be a three layer neural network with two hidden layers of size 100, 50, and activation function as eLU for each layer. The optimizer of is ADAM. We train with 500 epochs with batch size set as 128. Grid search is employed to tune learning rate and a regularization term for variance estimates.

DP: The MC-dropout is implemented according to <https://github.com/yaringal/DropoutUncertaintyExps>. The parameter length scale is set to be $1e-2$, and we tune over precision parameter τ and dropout rate with grid search. The model consists of a three layer neural network with hidden sizes 100, 50. The activation function is reLU. The optimizer of is based on ADAM with the default setting. The prediction of outcome is achieved by generating 1,000 posterior samples to estimate the first and second moment for the approximate Gaussian Distribution. We train with 300 epochs with batch size set as 128.

The second step, calibrated regression, (Kuleshov et al., 2018) is implemented by fitting the *interp1d* function from python scipy package with its default setting for less calibrated initial estimates. Note that the training data when involving calibration is further split into 7/3. 70 % of the data are used to retrain the model and the rest are used to form a recalibration mapping.

CQR: The conformalized quantile regression is implemented according to <https://github.com/yromano/cqr>. We use its built-in random forest model with default parameter tuning scheme and model specification. CQR can generate uncertainty interval for any specified nominal

level q at a time, but this is not scalable for the sketching of the full distribution, so we skip \hat{gof} evaluation for CQR. The conditional median estimate using CQR is achieved by first estimating the uncertainty interval of which the left and right limit correspond to the conditional 49.5 % and 50.5 % quantiles. Then we take their average to obtain an approximation of median.

C.2.2 PREPROCESSING

For the non-temporal UCI datasets (except energy), input arguments are all normalized covariate matrix. For energy data, the covariate of current time and the outcome of the previous observations are combined to predict the current outcome. For electronic health records data, the data is first discretized to month intervals. Missing data are imputed using carry-last-one-forward or the population mean if no value is available. To help with informative missingness, a binary indicator variable is augmented for each feature to mark whether the value is real or imputed. A second augmented variable is added to represent the time since last measurement for each feature. If a patient never had that feature measured previously, this value is set to 120, equivalent to 10 years. After these preprocessing steps, an LSTM is applied to the data using 40 hidden units. The LSTM is trained initially to predict a mean output as a dimension reduction procedure for the input feature space. Its missingness is imputed, but only the observed data contributed to the calculation of empirical loss. After pre-training the mean function, we use the predicted mean, the time since the last measurement and the last observed outcome measurement to constitute the three dimensional input space. Lastly, we combine observed data from all patients, which forms a long datasets.

Appendix D. Figures and Tables to Visualize Additional Datasets

In this section, we attach some other explorations and experiments on different data, that were not included in main article. They are the visualizations for calibration and sharpness for Energy, Crime and MPG data. In all three cases, CN-g is shown to generate both faithful and sharp uncertainty intervals.

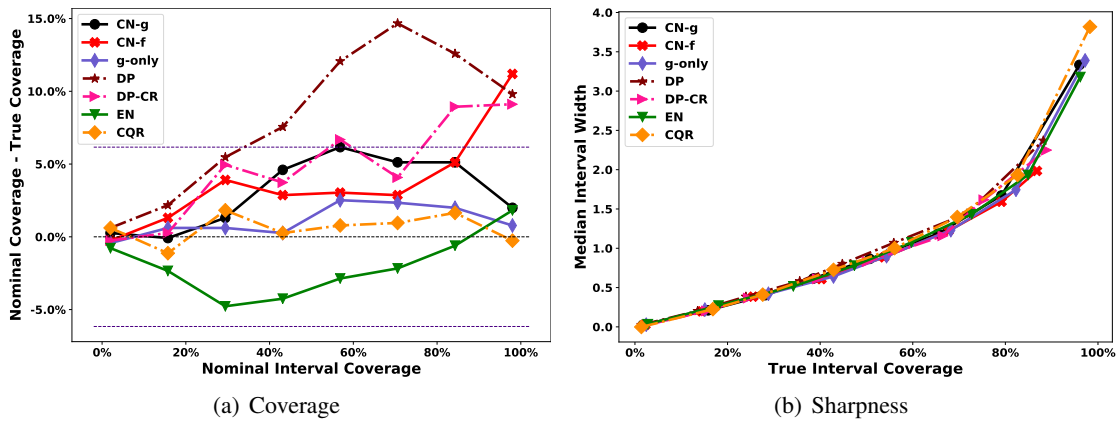


Figure S1: **Energy Data**, 1(a) shows the nominal coverage versus the difference between nominal coverage and empirical coverage for the Energy data with all methods, and CQR is visually more calibrated in this case; 1(b) evaluates the median interval width against the true interval coverage. All methods in this case present similar sharpness.

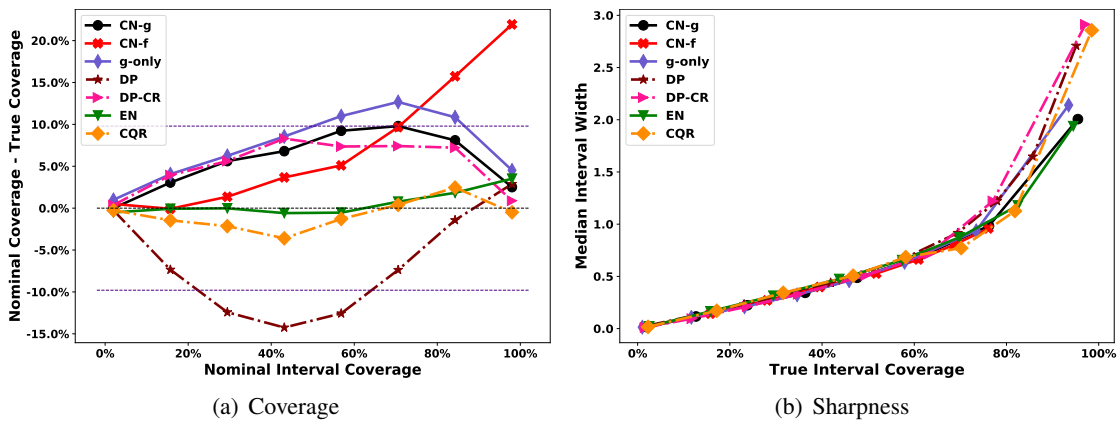


Figure S2: **Crime data**, 2(a) shows the nominal coverage versus the difference between the nominal coverage and the empirical coverage for the Crime data with all methods and EN is visually more calibrated in this case ; 2(b) evaluate the median interval width against the true interval coverage. CN and EN have overall better sharpness for higher empirical coverage levels.

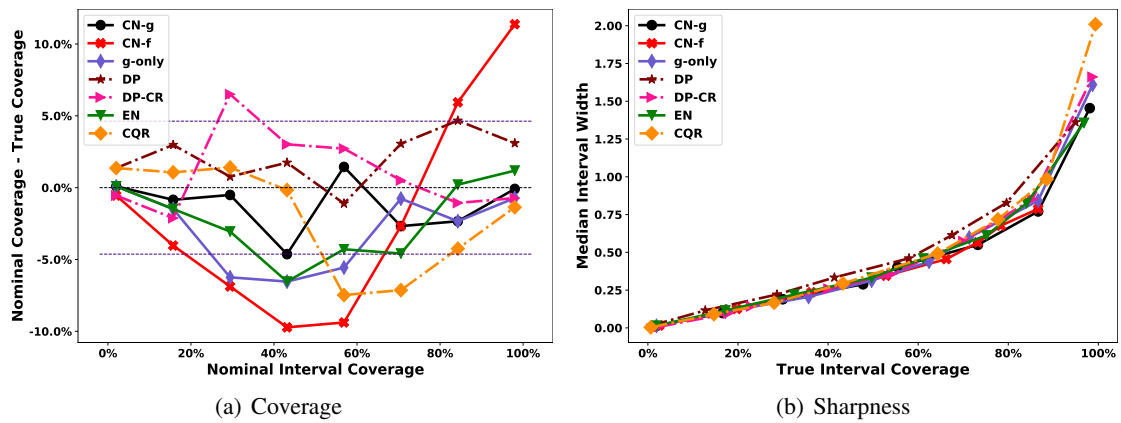


Figure S3: **MPG**, 3(a) shows the nominal coverage versus the difference between nominal coverage and empirical coverage for MPG data with all methods; 3(b) evaluates the median interval width against the true interval coverage. CN-g in this case overall has the best calibration and sharpness.